LASER BEAM WELDING OF AISI 316 STAINLESS STEEL IN MICROGRAVITY ENVIRONMENT -EXPERIMENTS ABOARD A KC-135 FLIGHT

By

Guoqing Wang

A thesis
presented to the University of Manitoba
in partial fulfilment of the requirements for the degree
of Master of Science in Mechanical Engineering

Winnipeg, Manitoba
August, 1993

ISBN 0-315-86095-2

Canada

Name GUOQING WANG

Dissertation Abstracts International is arranged by broad, general subject categories. Please select the one subject which most nearly describes the content of your dissertation. Enter the corresponding four-digit code in the spaces provided.

METALLURGY
SUBJECT TERM

0743
SUBJECT CODE

UMI

Subject Categories

THE HUMANITIES AND SOCIAL SCIENCES

COMMUNICATIONS AND THE ARTS
Architecture 0729
Art History 0377
Cinema 0900
Dance 0378
Fine Arts 0357
Information Science 0723
Journalism 0391
Library Science 0399
Mass Communications 0708
Music 0413
Speech Communication 0459
Theater 0465

EDUCATION
General 0515
Administration 0514
Adult and Continuing 0516
Agricultural 0517
Art 0273
Bilingual and Multicultural 0282
Business 0688
Community College 0275
Curriculum and Instruction 0727
Early Childhood 0518
Elementary 0524
Finance 0277
Guidance and Counseling 0519
Health 0680
Higher 0745
History of 0520
Home Economics 0278
Industrial 0521
Language and Literature 0279
Mathematics 0280
Music 0522
Philosophy of 0998
Physical 0523
Psychology 0525
Reading 0535
Religious 0527
Sciences 0714
Secondary 0533
Social Sciences 0534
Sociology of 0340
Special 0529
Teacher Training 0530
Technology 0710
Tests and Measurements 0288
Vocational 0747

LANGUAGE, LITERATURE AND LINGUISTICS
Language
- General 0679
- Ancient 0289
- Linguistics 0290
- Modern 0291

Literature
- General 0401
- Classical 0294
- Comparative 0295
- Medieval 0297
- Modern 0298
- African 0316
- American 0591
- Asian 0305
- Canadian (English) 0352
- Canadian (French) 0355
- English 0593
- Germanic 0311
- Latin American 0312
- Middle Eastern 0315
- Romance 0313
- Slavic and East European 0314

PHILOSOPHY, RELIGION AND THEOLOGY
Philosophy 0422
Religion
- General 0318
- Biblical Studies 0321
- Clergy 0319
- History of 0320
- Philosophy of 0322

Theology 0469

SOCIAL SCIENCES
American Studies 0323
Anthropology
- Archaeology 0324
- Cultural 0326
- Physical 0327

Business Administration
- General 0310
- Accounting 0272
- Banking 0770
- Management 0454
- Marketing 0338

Canadian Studies 0385
Economics
- General 0501
- Agricultural 0503
- Commerce-Business 0505
- Finance 0508
- History 0509
- Labor 0510
- Theory 0511

Folklore 0358
Geography 0366
Gerontology 0351
History
- General 0578
- Ancient 0579
- Medieval 0581
- Modern 0582
- Black 0328
- African 0331
- Asia, Australia and Oceania 0332
- Canadian 0334
- European 0335
- Latin American 0336
- Middle Eastern 0333
- United States 0337

History of Science 0585
Law 0398
Political Science
- General 0615
- International Law and Relations 0616
- Public Administration 0617

Recreation 0814
Social Work 0452
Sociology
- General 0626
- Criminology and Penology ... 0627
- Demography 0938
- Ethnic and Racial Studies 0631
- Individual and Family Studies 0628
- Industrial and Labor Relations 0629
- Public and Social Welfare 0630
- Social Structure and Development 0700
- Theory and Methods 0344

Transportation 0709
Urban and Regional Planning 0999
Women's Studies 0453

THE SCIENCES AND ENGINEERING

BIOLOGICAL SCIENCES
Agriculture
- General 0473
- Agronomy 0285
- Animal Culture and Nutrition 0475
- Animal Pathology 0476
- Food Science and Technology 0359
- Forestry and Wildlife 0478
- Plant Culture 0479
- Plant Pathology 0480
- Plant Physiology 0817
- Range Management 0777
- Wood Technology 0746

Biology
- General 0306
- Anatomy 0287
- Biostatistics 0308
- Botany 0309
- Cell 0379
- Ecology 0329
- Entomology 0353
- Genetics 0369
- Limnology 0793
- Microbiology 0410
- Molecular 0307
- Neuroscience 0317
- Oceanography 0416
- Physiology 0433
- Radiation 0821
- Veterinary Science 0778
- Zoology 0472

Biophysics
- General 0786
- Medical 0760

EARTH SCIENCES
Biogeochemistry 0425
Geochemistry 0996
Geodesy 0370
Geology 0372
Geophysics 0373
Hydrology 0388
Mineralogy 0411
Paleobotany 0345
Paleoecology 0426
Paleontology 0418
Paleozoology 0985
Palynology 0427
Physical Geography 0368
Physical Oceanography 0415

HEALTH AND ENVIRONMENTAL SCIENCES
Environmental Sciences 0768
Health Sciences
- General 0566
- Audiology 0300
- Chemotherapy 0992
- Dentistry 0567
- Education 0350
- Hospital Management 0769
- Human Development 0758
- Immunology 0982
- Medicine and Surgery 0564
- Mental Health 0347
- Nursing 0569
- Nutrition 0570
- Obstetrics and Gynecology .. 0380
- Occupational Health and Therapy 0354
- Ophthalmology 0381
- Pathology 0571
- Pharmacology 0419
- Pharmacy 0572
- Physical Therapy 0382
- Public Health 0573
- Radiology 0574
- Recreation 0575
- Speech Pathology 0460
- Toxicology 0383

Home Economics 0386

PHYSICAL SCIENCES
Pure Sciences
Chemistry
- General 0485
- Agricultural 0749
- Analytical 0486
- Biochemistry 0487
- Inorganic 0488
- Nuclear 0738
- Organic 0490
- Pharmaceutical 0491
- Physical 0494
- Polymer 0495
- Radiation 0754

Mathematics 0405
Physics
- General 0605
- Acoustics 0986
- Astronomy and Astrophysics 0606
- Atmospheric Science 0608
- Atomic 0748
- Electronics and Electricity 0607
- Elementary Particles and High Energy 0798
- Fluid and Plasma 0759
- Molecular 0609
- Nuclear 0610
- Optics 0752
- Radiation 0756
- Solid State 0611

Statistics 0463

Applied Sciences
Applied Mechanics 0346
Computer Science 0984
Engineering
- General 0537
- Aerospace 0538
- Agricultural 0539
- Automotive 0540
- Biomedical 0541
- Chemical 0542
- Civil 0543
- Electronics and Electrical 0544
- Heat and Thermodynamics ... 0348
- Hydraulic 0545
- Industrial 0546
- Marine 0547
- Materials Science 0794
- Mechanical 0548
- Metallurgy 0743
- Mining 0551
- Nuclear 0552
- Packaging 0549
- Petroleum 0765
- Sanitary and Municipal 0554
- System Science 0790

Geotechnology 0428
Operations Research 0796
Plastics Technology 0795
Textile Technology 0994

PSYCHOLOGY
General 0621
Behavioral 0384
Clinical 0622
Developmental 0620
Experimental 0623
Industrial 0624
Personality 0625
Physiological 0989
Psychobiology 0349
Psychometrics 0632
Social 0451

LASER BEAM WELDING OF AISI 316 STAINLESS STEEL IN MICROGRAVITY ENVIRONMENT -EXPERIMENTS ABOARD A KC-135 FLIGHT

BY

GUOQING WANG

A Thesis submitted to the Faculty of Graduate Studies of the University of Manitoba in partial fulfillment of the requirements for the degree of

MASTER OF SCIENCE

ABSTRACT

Low power(70W) continuous wave CO_2 laser welding under microgravity was conducted during a KC-135 parabolic flight. The welding experiments were performed on thin 316 stainless steel strips. The welding parameters were optimized first in the ground base tests and then continuous welding was conducted during the periods of changing gravity level on board the KC-135. The weld microstructure characteristics were examined using optical and scanning electron microscope. During the absence of gravity, wider weld width and deeper penetration were found to occur. The weld was characterized by dispersed entrapped slag, porosity and suspended weld particles which may lead to a weak joint in real space welding.

ACKNOWLEDGEMENTS

I wish to take this opportunity to thank Dr. K. N. Tandon, not only for his supervision and guidance, but also for his encouragement and motivation during the course of this investigation. I would also like to acknowledge the invaluable technical assistance of Mr. John VanDorp, Mr. Don Mardis and Mr. Lincoln Oree in this work.

The financial support to this work by Canadian Space Agency is gratefully acknowledged. The recognition should also be given to the MPB Technology Inc. and University of Waterloo (Prof. W. W. Duley and Mr. M. Olfert) for providing the opportunity to use their equipment and the technical support for its operation.

TABLE OF CONTENTS

LIST OF FIGURES

LIST OF TABLES

CHAPTER 1

INTRODUCTION

The 21th century offers a great challenge to today's science and technology for the exploration of the frontiers of space. A unique part of this challenge will be the fabrication of structures in this unusual environment. For construction in space, major efforts have been initiated to develop new materials which will have the required properties for the space environment. A major consideration of joining these materials in original construction or during repair events is under development. Among those joining methods, laser welding shows great promise.

Laser beam welding is becoming a commercially important technology in today's space industry. The unique environment in space is mainly characterised by very low gravitation, or microgravity, up to 10^{-4}g, and high vacuum. In recent years, the interest of studying laser welding under microgravity conditions has increased dramatically [1-6]. Research on the effects of microgravity on welding was first conducted by the former Soviet Union, some 20 years ago. Three welding processes: fusible electrode welding, low-pressure plasma welding and electron beam welding, were explored on aluminum alloys, titanium alloy and stainless steel, respectively [1]. Problems existed with the first two processes due to instability of the arc in vacuum, while electron beam welding showed promise.

Laser welding can be regarded as similar to electron beam welding. High density energy is used to heat and fuse the mating surfaces together. The choice of the laser as a welding source in a space application comes from the consideration of possibility of getting solar energy to pump the laser in space, and laser can not only be execute in outer space, but can also be conducted inside the pressurized module should this processing is needed. This is a unique advantage of laser welding over electron beam welding which is difficult to be performed in a gas environment.

To date, only a few laser welding experiments in a stimulated microgravity environment have been tried in last few years [4-7]. But in terms of weld metallurgy, the effect of microgravity on weld microstructure and composition change in simulated or real space welding experiments is yet to be made clear. To explore the feasibility of metal welding in space and study its weld characteristics, the Canadian Space Agency sponsored a microgravity laser welding program in which several laser welding experiments on stainless steel were flown on board the KC-135 using a 120 watt continuous wave, carbon dioxide laser materials processing system. It is hoped that the understanding of microgravity effects on laser welding process will help in the development of space exploration in the future.

CHAPTER 2

LITERATURE REVIEW

2.1 Laser and laser welding

The laser, which stands for "Light Amplification by Stimulated Emission of Radiation", is a device that emits a highly coherent, monochromatic beam of electromagnetic radiation. Laser action was predicted in theory by Townes and Schawliw in 1958, and became a reality in the summer of 1960 when Dr. T. H. Maiman, of Hughes Research Laboratories, demonstrated emission of coherent light radiation in a ruby laser. Since then, laser technology has advanced at a tremendous rate. This advent of a high energy intensity surface heating sources is having a strong impact on the field of materials processing. Since the 1960's, The laser has been used as energy for welding. Many researches have been conducted on various laser beam welding experiments [8-13].

Laser beam welding (LBW) is distinguished from electron beam welding (EBW) which only operates in a vacuum environment. It can be used to join thick-to-thin metals or dissimilar metals easily. There is no discernible temperature rise in areas adjacent to laser beam impact, thus welding can be close to heat-sensitive materials. It requires no vacuum chamber, and the laser beam can be transmitted through air for appreciable distances without serious power degradation. The non-contact process of LBW eliminates mechanical distortion of workpieces, particularly when welding thin sheet. As a special heat source, a modest power laser can provide an energy density up to $10^8 W/cm^2$

whereas the arc welding at 200A and 20V can only provide $5x10^3 w/cm^2$ [14].

2.1.1 Components of a laser welding system

There are three fundamental parts in a laser which include a laser material or medium, a method of excitation and a resonant cavity. Fig.2.1 schematically illustrates the principle of a laser welding system. The resonant cavity is formed by two precisely oriented mirrors, one of which is slightly transparent. An active medium, which may be either a gas or a crystal doped by certain atoms (such as chromium in the ruby), is placed between the mirrors.

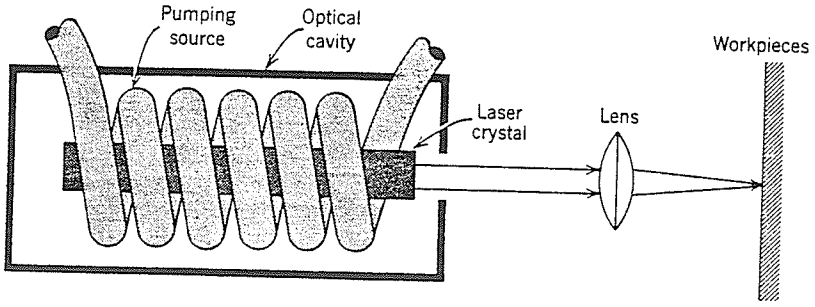

Fig.2.1 A typical laser welding system [17].

The medium must possess two atomic states separated in energy by an amount corresponding to the frequency desired, and it must be possible to overpopulate the upper of these states with respect to the lower. This is done by "pumping" the atom from a ground state to a higher energy state either electrically or optically. From the upper state some atoms decay spontaneously to the lower state and emit light which is incoherent and

is radiated in all directions at random. In the presence of the resonant cavity, however, some of this spontaneous emission excites one of the resonant modes of the cavity, and then induces emission in the medium. When the interaction is strong enough, coherent electromagnetic waves build up. Some of these come put through the partially transparent mirror forming one end of cavity and emerges as a sharply defined beam of coherent light--laser.

2.1.2 Classification of lasers

Industrial lasers used for material processing and welding can be divided into two categories: solid state and gas, depending on the lasing medium. Correspondently, solid-state lasers have a wavelength of 1.06μm, whereas gas lasers have a wavelength of 10.6μm [15].

Solid-state lasers are characterized by an active medium of an impurity in some host material. For material processing, the dopant is the Neodymium ion (Nd^{+++}) in either glass or YAG (Yttrium aluminum garnet which has the chemical composition $Y_3Al_5O_{12}$). The excitation is by means of intense optical lamps (Krypton or xenon). Depending on the excitation method, the output characteristics of Nd:YAG lasers may be continuous or repetitively pulsed. In continuous operation, the average power of laser varies from the order of 10W to the order of 100W or more, depending on the transverse electric and magnetic (TEM_{mn}) modes, where subscripts m and n specify the integral number of transverse modal lines across the laser beam. The simplest mode is TEM_{00} in which the

flux density over the beam cross section is approximately Gaussian and this beam is the most focusable. Other modes are called multimode, in general. For repetitively pulsed lasers, the average output also changes dramatically.

The most efficient gas laser currently available for material processing is the CO_2 laser, which can be utilized in both the high-power continuous wave and pulsed operating modes. Carbon dioxide lasers use an electric discharge as the source for exciting the lasing medium--CO_2 gas molecule mixed with some helium and nitrogen. It can be further classified according to their gas flow system. The simplest CO_2 laser, which has an axial-flow system, is capable of generating a laser beam with a continuous power rating from 50 to 1000W.

2.1.3 Laser welding applications

Laser welding application has been rapidly developing in the areas of automotive, electronics and aerospace industries. Lots of materials has been successfully welded by LBW, including ferrous and non-ferrous metals [11-13,16]. The welding potential of lasers has also been demonstrated on some other of the more difficult to join metals, for example, columbium, and molybdenum [17].

But LBW also have certain limitations at the present time. One important shortcoming when compared with the EBW process is that EBW can weld extremely thick sections, whereas lasers can't. Current capabilities in material thickness that can be welded are

25mm maximum in single pass [18]. Also current costs for welding, compared with conventional methods are moderately high. Therefore, the most promising application for LBW will be in exotic space.

The laser selection will be based on the welding purposes. Generally there are two kinds of industrial laser welding process--conduction limited and deep penetration as shown in Fig.2.2. In former,the laser beam energy is delivered to the metal through the depth of the weld, not just to the top surface, It requires a high-power CO_2 laser (Fig.2.2(a)). In later case, the metal absorbs the laser beam at the work surface, the subsurface region is heated entirely by thermal conduction, often solid-state and moderate power CO_2 lasers are used.

2.1.4 Laser Beam-material interactions

When the laser beam interacts with a material, part of the energy of the laser beam is absorbed by the material and the rest of it is reflected . The properties of the laser beam and material will affect this interaction [19-26].

To understand these interactions between beam and material is difficult, since many of the dominant physical effects occur during laser processing of metals with a CO_2 laser. In a study of physical phenomena within laser-induced keyholes conducted by W.W.Duley by using a low power CO_2 laser, an attempt has been made to describe this interaction at the sample surface [27]. It was found that the surface condition (such as roughness),

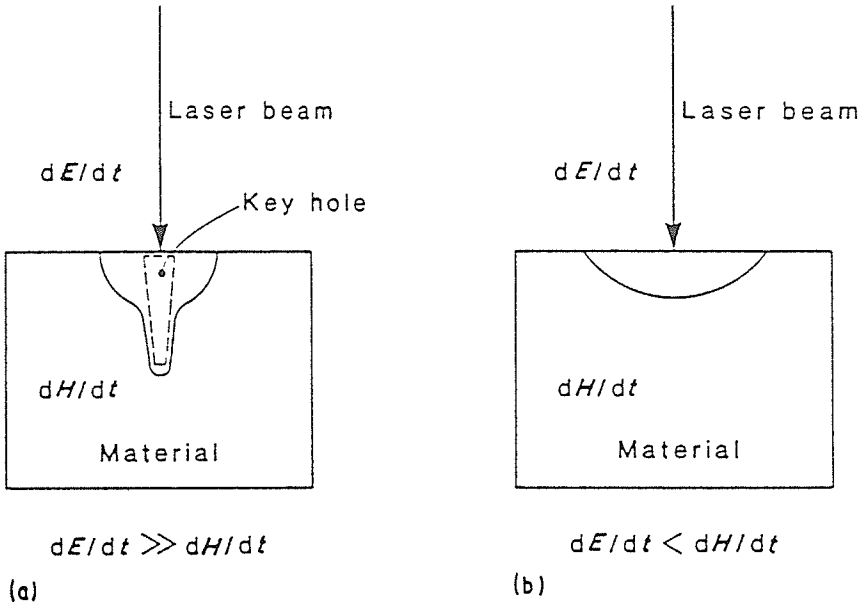

Fig.2.2 Schematic representation of

(a) deep penetration and (b) conduction welds[13].

is an important factor determining the fraction of incident radiation that is retained as heat. Then heat is transferred within the substrate. At sufficiently high heating rates the surface begins melting while temperature keeps going up until vaporization occurs. At this time, the melt is flowing away from the area of the beam focus due to surface tension in the melt and the pressure caused by evaporating gas. As the heating continues, eventually a keyhole is formed.

In the discussion of the interaction between laser beam and vapour evolved from a

keyhole, it is believed that a plasma is formed there which transiently prevents the beam reaching the workpiece [28-32]. P.G.Klemans regards the melting around the keyhole resulted from absorption of beam radiation in the plasma within the keyhole and reradiated to the walls around [27].

2.1.5 Laser welding of stainless steels

Stainless steel can be broadly classified as martensitic, ferritic, austenitic, precipitation hardening and duplex. Most stainless steels are readily weldable provided proper precautions are taken. For different classes of stainless steels each have different weldability problems. For example, martensitic stainless steels are more susceptible to hydrogen-induced cracking, while the austenitic grades are more prone to solidification cracking [33, 34]. The austenitic stainless steels are the most widely used grades and many studies have been carried out on its weldability [34].

There are two features of stainless steels which have a strong influence on welding behaviour. Firstly, the low thermal conductivity (only half of low alloy steels) requires a lower nominal heat input, and the high levels of easily oxidizable alloying elements, such as Cr, which requires the weld pool to be carefully protected during welding operations [35]. Secondly, stainless steels are primarily used in corrosion resistant applications. Hence, its corrosion resistance at the weld and HAZ should be preserved.

The majority of stainless steels are welded using arc processes, such as TIG (Tungsten-

Inert-Gas), MIG (Metal-Inert-Gas). Much welding of stainless steel has applied to relatively thin sections (<13mm thick). However, thicker sections, such as those required for pressure vessel manufacture used in oil and nuclear industries, have been also attempted for high productivity using electron beam or laser beam welding.

Laser beam welding is one of the high-energy density welding processes which produce narrow weld bead profiles and offer exceptional deep penetration capabilities. Aristotile and Poli compared laser and TIG weld quality when fabricating 1.5-3mm thick AISI 304 and AISI316 stainless steels [36]. The mechanical properties of laser welds were similar to those in TIG welding but the corrosion resistance was superior. Similar results were also observed by Koso by using a 5KW CO_2 laser in the welding of AISI304 pipe [37]. Weld metal properties were equivalent to those of the base material.

Some parameters for laser welding of 300 series stainless steel are given in Fig.2.3. Here, the penetration is plotted as a function of welding speed for various low-power laser welding, both pulsed and continuous [15]. We can see that for welding speeds of 20 to 60 in/min, the 150W pulsed Nd:YAG laser can weld thicker sections than the 400W continuous wave Nd:YAG laser. And below 120 in/min, the 400W pulsed Nd:YAG laser welds thicker sections than the 375W continuous wave CO_2 laser at the same welding speed, but above 120 in/min the 375W CW CO_2 laser welds the same thickness as the 400W pulsed Nd:YAG laser at the same speed. The 400W pulsed Nd:YAG laser operating at 200 PPS (pulses per second) can make a penetration weld.

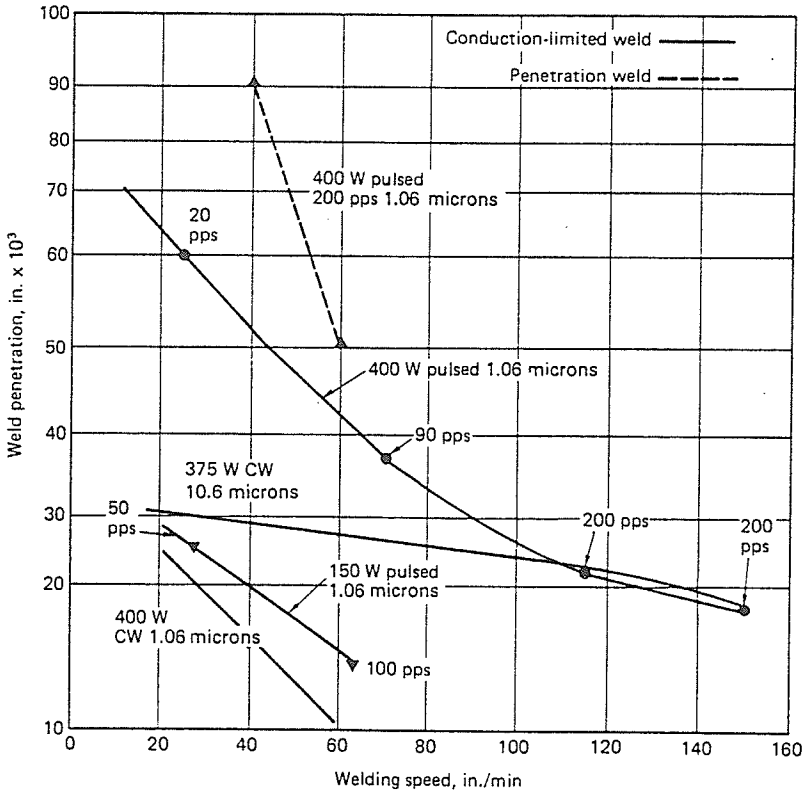

Fig.2.3 Effect of welding speed on penetration in a 300 series stainless steel [15].

Holbert and Mustaleske investigated three laser welding processes (pulsed Nd:YAG, pulsed CO_2 and continuous wave CO_2) for 0.01in thick 316 stainless steel butt welding, and got very good penetration, but porosity was noted in the weld [8]. With the pulsed Nd:YAG, the porosity increased as the penetration increased while the power varied from 24 to 35 watts (Fig.2.4). But the CW CO_2 laser welding obtained a weld with virtually no porosity while the power changed from 242W to 430W. The explanation for porosity was given by author, that the porosity in the weld was part of the metal vapour

established when the beam was heating by keyhole instead of by conduction. This research concluded that CW CO_2 laser heating by conduction was one of the most promising techniques to get a porosity-free weld.

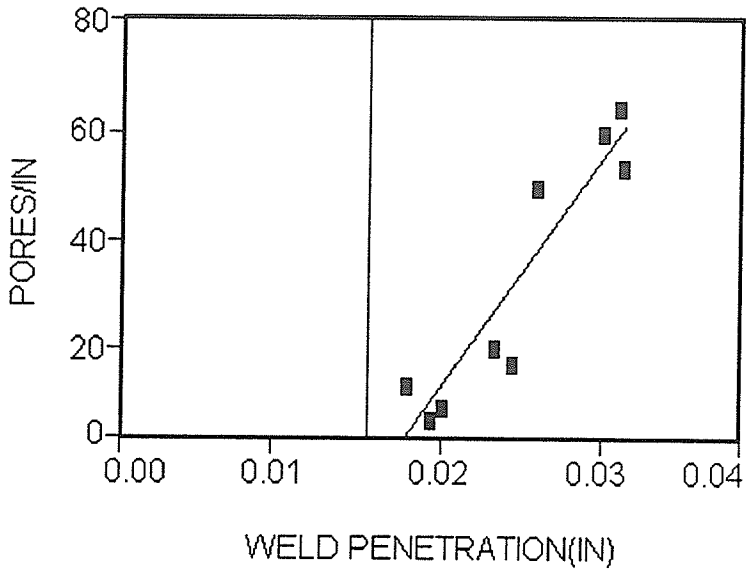

Fig.2.4 The relationship between porosity and penetration in pulsed Nd:YAG laser [8].

High power laser welding of stainless steel is part of the research by Boussean and Signamarcheix [39]. A 5KW laser of multimode and 800W single-mode laser device was used to weld 2-10mm sample. The melting zone during welding was protected with helium or argon gas. It was found that a greater penetration is obtained using helium as the protection gas. This difference is credited to the increased plasma which develops above the melt zone when using argon, because the absorption of energy considerably reduces the penetration. It was also found that welding power and speed have

counteracting effects on the geometry of the bead. The study of the relationship between P/V (energy applied per unit of length) and penetration depth shows that for low P/V values the penetration is small. Above a threshold value of P/V, the depth to which can be welded rapidly increases, then additional energy will only increase the width of the bead.

2.2 Welding in space and its development

2.2.1 Microgravity and material processing

Aiming to develop space as a national resource, the research on microgravity science has been conducting in America , the former Soviet Union and other countries in Europe (including Germany, Sweden, France) since the 1950's. About 60 universities and 10 industrial labs in US are involved in the microgravity science research led by the office of Space Science and Application in NASA. Most of the current research is related to the effects of reduced gravity which is a significant characteristic of the space environment. The advantages of this environment include reduced or eliminated buoyancy driven convection, elimination of sedimentation and elimination of hydrostatic pressures.

Extensive amount of basic and applied research on microgravity is now being conducted [41-48]. One of the important programs is the study of fluid dynamics and mass transport phenomena under the condition of microgravity. Research of crystal growth of electronic materials and metals is also of great interest. Some experiments, such as the growth of protein crystals in space, have indicated that a higher resolution of the crystal structure

may be obtainable from space-growth crystals [46]. X-ray diffraction studies showed that the space crystal was macroscopically much more homogeneous than the earth-grown crystal. Since dispersions during metal crystallizing do not settle as rapidly in microgavity as they do in unit gravity. Processing of homogeneous composite materials in space shows some promise [49].

It has been observed that the gravity force has apparent effects on the vertical directional solidification of light, solute rejecting alloys [50, 51]. During the dendritic solidification of this alloy in normal gravity environment, a solute rich layer develops in front of the interface and within the solid-liquid mushy zone. Since the solute is lighter than the bulk liquid, the least dense liquid is therefore located at the base of the mushy zone, which results in convective phenomena such as freckling, fingering and pluming. This could be eliminated or at least reduced when solidification is performed in decreased gravity level, as reported by McCay.

Facilities currently used to study microgravity science include drop tubes/towers that give up to about 5 seconds of low gravity, KC-135 parabolic flights which give 20-30s of low gravity, and space shuttle flights which can be used to carry out various experiments during a single flight. Future shuttle flying will be more convenient way to do this research. NASA is planning to build a space station to provide a microgravity research laboratory and a test bed for commercial materials processing in space.

2.2.2 Welding technology in space and its developments

The 21th century offers a great challenge to the science researcher for space exploration. According to the U.S. space exploration strategy, with the development of the earth-constructed transport vehicle, an advanced space station, Freedom, has been scheduled for construction in orbit in the near future. This will serve as the first space port. From the space station new transfer vehicles which are different from the ones fabricated on earth, will be constructed for deeper space exploration, such as the moon and Mars. For construction in space, many new materials which have the required properties for the space environment have been developed including their welding on earth. But joining these materials in this unusual environment remains unsolved according to the review of published literature. Further study is still needed before a large structure could be fabricated or repaired in space using welding techniques.

The potential value of welding in space for maintenance, repair and fabrication of structures in space was recognized by scientists in the 1960's. A variety of joining processes had been considered to be employed for space welding, Table 2.1 gives a comparison for these methods based on several issues.

A) Electron beam welding

The earliest efforts to develop capabilities for welding in space began at the E.O. Paton welding Institute, located in Kiev, in 1965. Electron Beam welding was one of three candidate welding processes explored by them because of its inherent compatibility with

a vacuum environment. Fig.2.6 schematically illustrates the EBW process. The weld is created by the bombardment of a finely focused, high energy stream of electrons onto the workpiece. To avoid loss of the kinetic energy of the accelerated electron beam through collision with air molecules, welding is performed in a vacuum chamber in terrestrial applications. One drawback of this process is that the X-rays are generated when the electron beam strikes the workpiece.

With the EB welding, various metals including stainless steel, aluminum alloys and titanium alloys have been welded in low gravitational environment in a Russian program. Initial trials were conducted using equipment installed in a aircraft. A constant beam power of 1KW , beam current of 70 mA and welding speed of 30 m/min were employed. No major differences have been reported between samples welded on earth and those produced during a short-term flight simulating a micro-gravity environment [52]. This work has now been further extended to develop a "multipurpose work tool" based on a hand-held EB gun of 1KW power which has been used in space in 1984 welding steel, aluminum, and titanium alloys up to 3 mm thick. New space welding electron beam equipment for 1.5KW and 3KW capacities has been developed by Soviets since then. This will open considerably wider space construction options. In other electron beam welding efforts a European firm, Babcock Power Ltd., is developing an EBW device for in-space welding of tubes. This system is ideally designed for automated welding which could reduce some EVA time.

Table 2.1 Welding processes and related issues of concern for space applications

ISSUE	PROCESS						
	BRAZING	RESISTANCE WELDING	GMAW	PAW	LASER WELDING	ELECTRON-BEAM WELDING	GTAW
IVA	Possible	Possible	Yes	Possible	Possible	No	Yes
EVA	Possible	Possible	No	Possible	Possible	Yes	Yes
Quality	Medium	Medium	Medium	High	High	High	High
Efficiency	Low	Medium	Medium	High	Very Low	Very High	High
Versatility	Limited	Limited	Fair	High	Moderate	Limited to EVA	Very High
Automation	Possible	Usually	Possible	Possible	Generally	Generally	Possible
Radiation (Penetrating)	None	None	None	None	None	Personnel Sheilding for X-ray	None
Radiation (Optical)	None	None	Eye Protec-tion req'd	Eye Protec-tion req'd	Eye Protec-req'd	No	Eye Protec-tion req'd
Inspectability	Poor	Poor	Component dependent	Component dependent	Component dependent	Component dependent	Component dependent
Other Advantages	Demonstrated on orbit				High D/W ratio	High D/W ratio	-Fit-up tolerant -Process control possible
Other Disadvantages		Two-side access req'd		Key hole close-out	-Manipulation -Limited fit-up constraints	-Vacuum req'd -Magnetic deflection	Inert gas require-

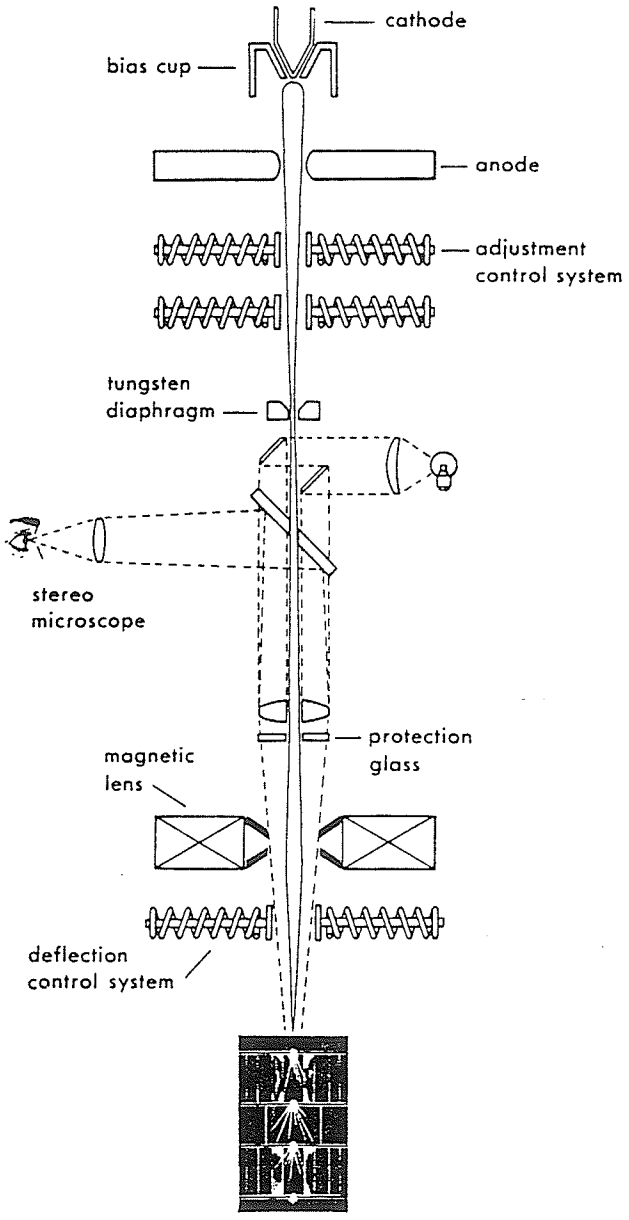

Fig.2.6 Schematic representation of electron beam welding [17].

B) Arc welding

The arc welding processes, so far used in space program, include consumable electrode welding (MIG) and plasma arc welding. Fig.2.7 schematically illustrates these two processes. In MIG welding the arc is struck between the workpiece and the electrode which can be continuously fed through the arc into the weld pool. On ground base process, the entire weld area is protected from atmospheric contamination by an inert gas shielding. Under the space conditions, the gas only provides the function of ionizing to form a plasma through which the current and heat of the arc are carried. The most significant problem encountered with this process is maintenance of arc stability in a vacuum circumstance. A recent effort has been made to solve this problem [53]. A modified gas tungsten arc welding torch which argon gas used for the arc plasma is fed through a hollow tungsten electrode instead of normal solid one was developed. This arrangement provides positive arc stabilization in vacuum environments. No shielding gas is required.

In plasma welding process, the arc is struck between a non-consumable electrode and an electrical conductive collect surrounding the electrode. Then ionizing the fluid gas to form a superheated plasma jet stream to heat the workpiece. In space condition, the shielding gas is not necessary. But the problems with arc stability exist.

C) Other metals joining techniques

Exothermic brazing experiments were conducted during the Skylab 1 mission. Welding

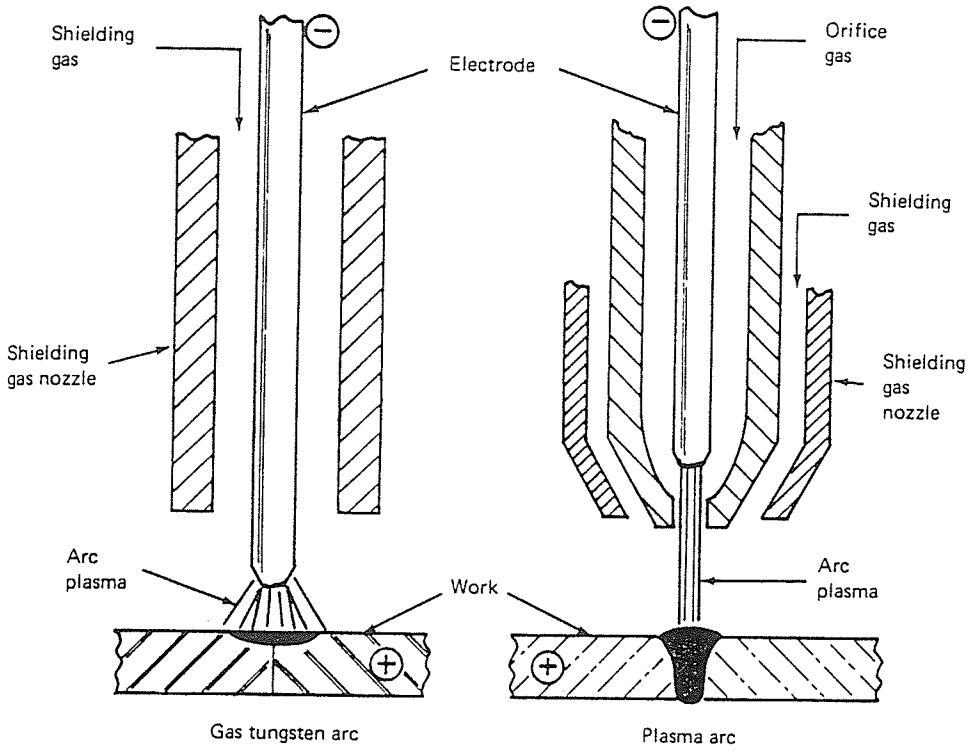

Fig.2.7 Schematic representation of

(a) gas metal-arc welding and (b) plasma-arc welding.

materials were 304L stainless steel and pure nickel. The braze employed was a near eutectic silver-copper alloy. The braze alloy flow and dispersion patterns found in these experiments were compared with those obtained on earth. It was found that a greater dispersion of braze was found. And porosity was observed also. But an obvious drawback of this process is the low strength of the weld joints [53].

In the early seventies, solar energy welding in space was attempted by the former Soviet

Union. A special apparatus was developed for this purpose [1]. Experimental tests showed that at normal radiation intensity in space of 0.145W/cm^2, the apparatus can give 1900W/cm^2 at the focal spot which is sufficient for welding and cutting of 0.2mm thickness sheets of high-temperature alloys. Using this method attempts have been made to weld aluminium alloys in 1981 without success due to the high optical reflectivity of the surface and high thermal conductivity.

D) Laser welding in space

Laser application expanded rapidly during last 20 years. Many traditional techniques of material processing, including surface treating, drilling, cutting, welding have been replaced by lasers. Due to its easy control and high energy density while without x-ray radiation compared with Electron beam, Laser is naturally considered an important techniques to be applied in repair and construction in space.

Conventional terrestrial studies of laser beam welding divided LBW into two groups as conduction welding or penetration welding with continuous wave or pulsed laser radiation. Comparatively, a CW penetration LBW has gain more interests of researchers for the study of welding in space since the pulsed LBW may induce mask effect and make the study complicate [4-7, 26, 52]. In recent years, Duley has performed experiments in low gravity using laser to melt polymers. By doing so they were trying to observe the dynamics in the keyhole and to explain the mechanisms responsible for the formation of porosity [26]. Simulated laser welding in space is also conducted by a research group in

University of Alabama in USA. The varying of weld morphology with the change of gravity level has been observed [4, 5]. But in terms of weld metallurgy, the effect of microgravity on weld microstructure or composition change is yet to be made clear.

2.3 Weld microstructure of the laser welded stainless steels

The chemical composition of the stainless steel weld is an important factor determining the weld microstructure [54]. A ratio of Cr_{eq}/Ni_{eq} was often used to predict the weld microstructure, as in Schaeffler diagram which was developed to describe the relationship between the compositions and microstructure of the stainless steel weld (Fig.2.8). When the Cr_{eq}/Ni_{eq} was high, the weld structure often consisted of ferrite (δ) surrounded by austenitic (γ). Low ratio will give rise to ferrite embedded in an austenitic matrix. The ferrite become coarser with an increase in the total sum of the alloying elements, i.e. the sum of $Cr_{eq}+ Ni_{eq}$.

However, the weld morphology is mainly determined by solidification process, which consisted of nucleation and growth processes [55-64]. The actual temperature gradient in the weld liquid is depicted in Fig.2.9. It can be seen that there is a region within which the actual temperature is less than the effective liquidus temperature due to the constitutional supercooling. In general, the extent of constitutional supercooling depends on both the temperature gradient in the weld liquid, G, and the rate of growth, R. A change in G changes the location of the intersection with the effective liquidus. An increase in R dictates a decreased time for diffusion in the weld liquid and thus a steeper

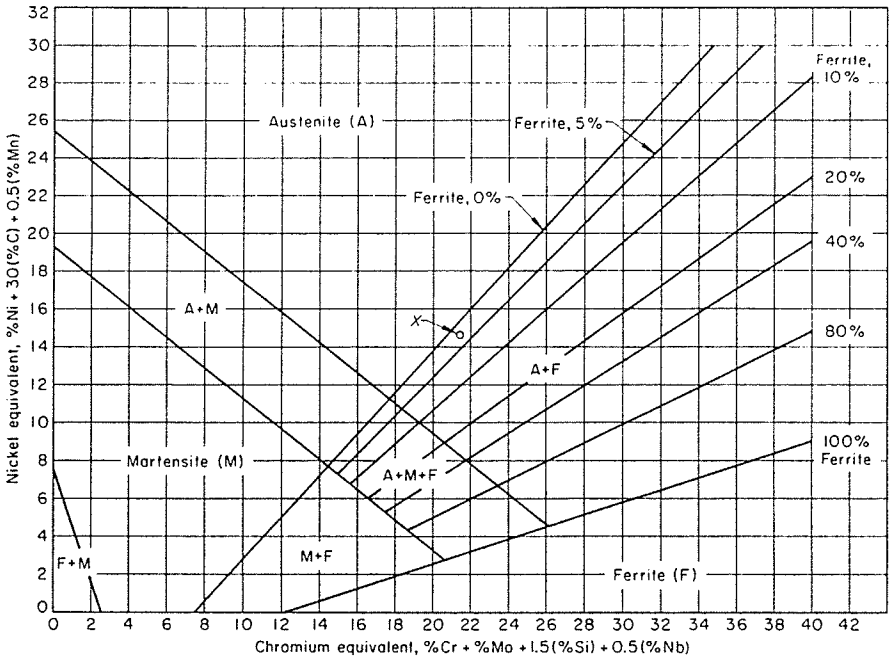

Fig.2.8 Schaeffler diagram [62].

concentration gradient must occur in the liquid near the solid-liquid interface. When the extent of the constitutional supercooling is small, a cellular structure results. On the other hand, if the constitutional supercooling becomes sufficiently great, a dendritic structure is formed as indicated in Fig.2.10. Because the constitutional supercooling depends on G and R, a relationship exist between the weld microstructure mode and G, R as illustrated in Fig.2.11. Note that low values of $G/R^{1/2}$ indicate an increased tendency for constitutional supercooling, thus favouring the dendritic mode of solidification. On the other hand, steep temperature gradients in the weld liquid and slow growth rates favour cellular growth.

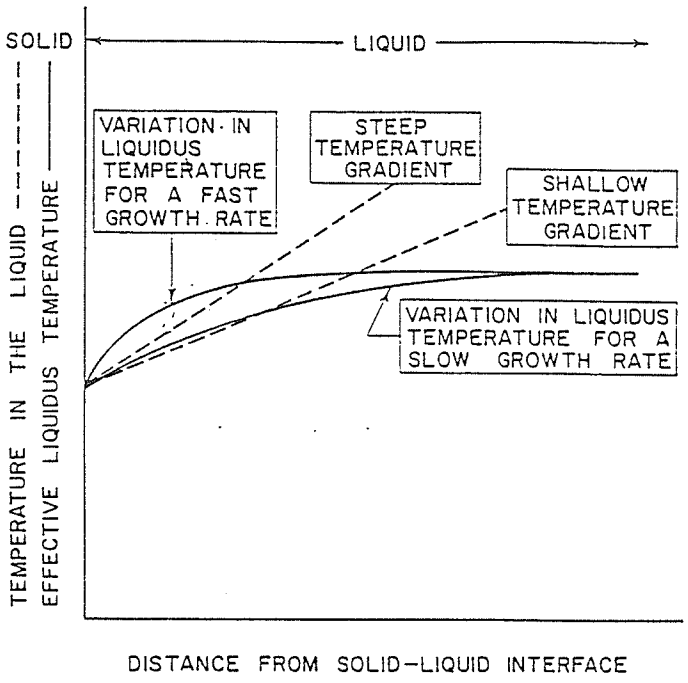

Fig.2.9 Effect of growth rate and temperature gradient on constitutional supercooling[55].

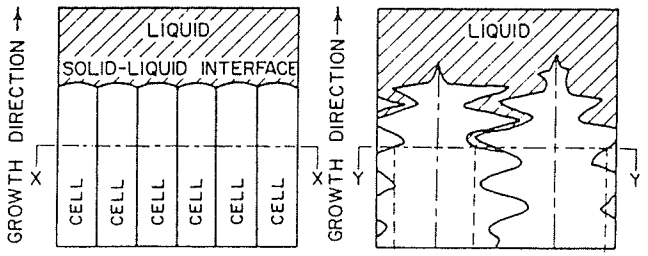

Fig.2.10 Schematic of cellular and dendritic growth patterns [55].

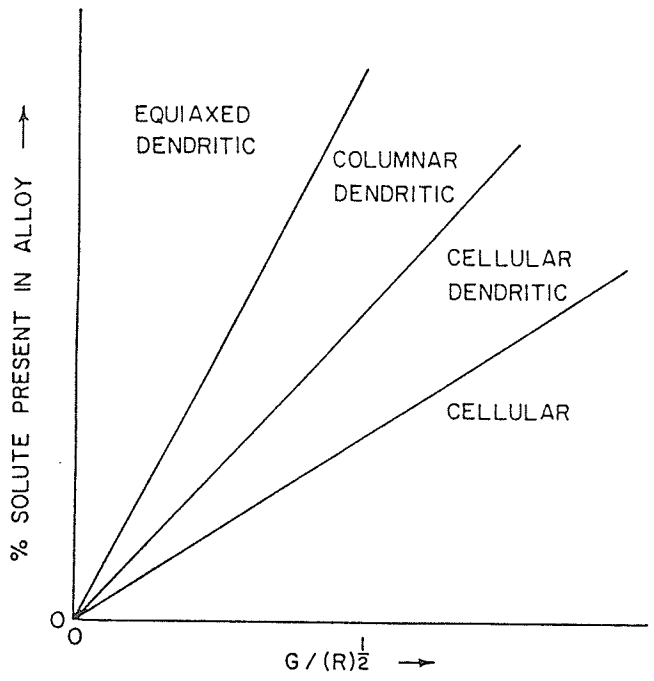

Fig.2.11 Schematic representation of the influence of growth rate R and the temperature gradient G on the pattern of solidification.

Since growth in weld is epitaxial [62-64], the growth process in the fusion zone is obviously influenced by the orientation of the grains in the base metal at the solid-liquid interface. Solidification studies of TIG welding of silicon iron with an average grain diameter of 5mm have indicated that, the relatively large base metal grain size produced a correspondingly large grain size in the fusion zone [54]. Chalmers has confirmed that dendritic growth in BCC materials tends to occur in the <100> direction [63]. Thus growth in weld fusion zone should therefore be easiest when the thermal gradient is parallel to this favoured direction. This results in competitive grain growth as shown in Fig.2.12. If competitive growth of columnar grains proceeds all the way to the weld

centerline, the weld metal will exhibit a fully columnar grain structure. However, in many materials, new grains can nucleate in the weld pool ahead of the growing columnar grains and block them off. The nucleation of such new grains will result in the formation of equiaxed grains in the center of the fusion zone. Certainly the formation of

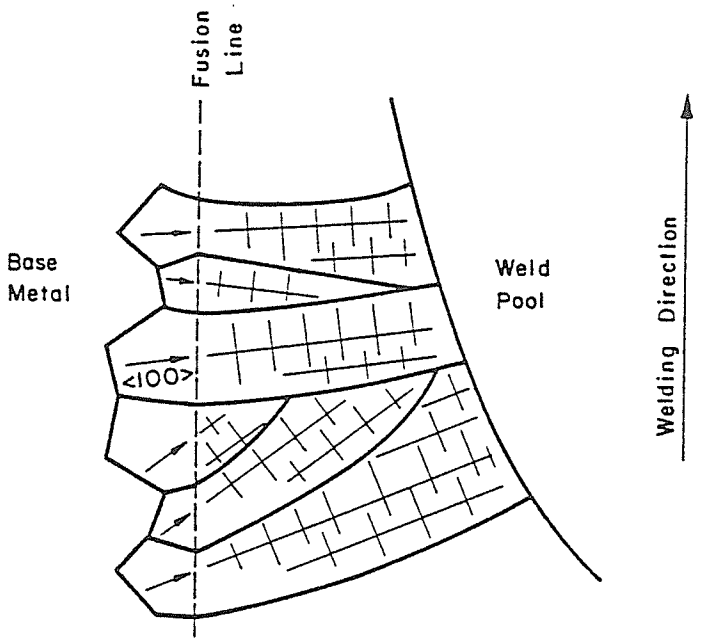

Fig.2.12 Epitaxial growth from the fusion line and competitive growth in the bulk weld metal [64].

equiaxed grains has other mechanisms, such as dendrite fragmentation and grain detachment, due to the significant convection in the weld pool [65]. However, in laser welding or other high energy intensity welding, dendrite fragmentation is unlikely to occur due to a very small weld pool.

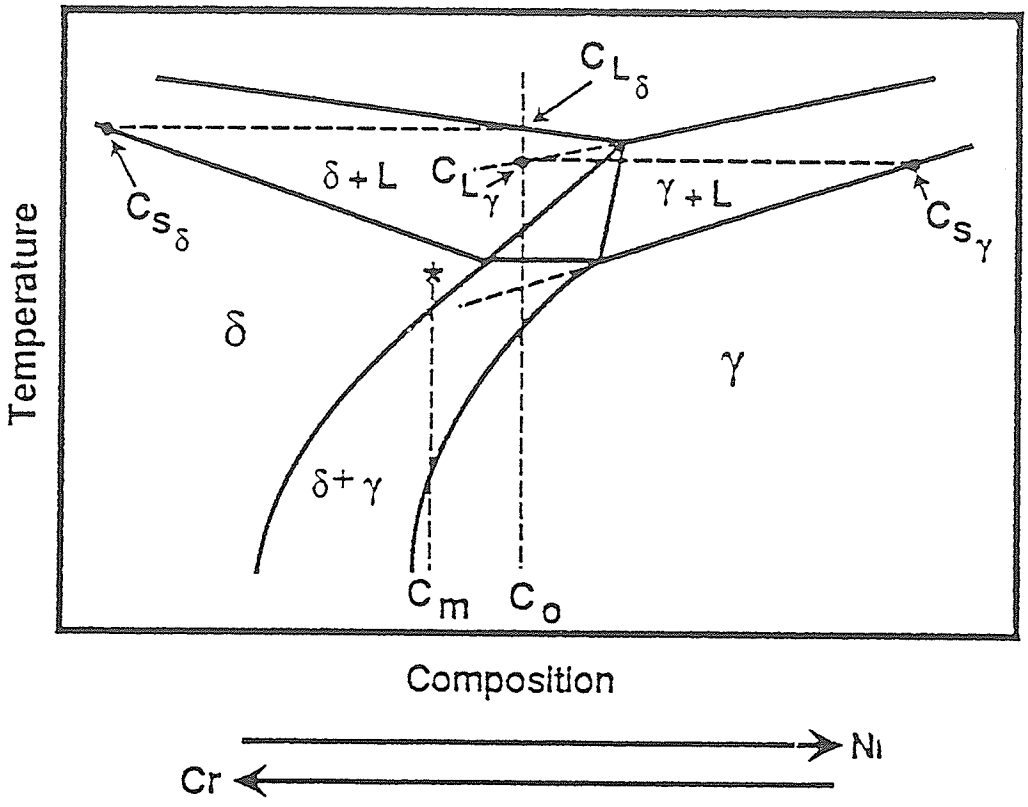

Fig.2.13 Schematic of a constant Fe vertical section [67].

Due to the high intensity heat input (10^{10}-10^{12}w/m^2) in laser welding, the cooling rate within the weld pool could reach as high as $5x10^3$ $^oC/S$ [66]. As a consequence, some unique features may arise during the solidification of laser weld. An important phenomenon happened in laser welding of stainless steels, particularly in austenitic stainless steels, is the formation of nonequilibrium phases [13, 66, 67]. It has been observed that the rapid cooling of the laser weld results in a reduction in the δ phase, while the γ increases. This may indicates that under the high cooling rate within the laser weld pool the primary austenite solidification is more favoured than the ferrite. By

examining the electron beam welding of 19Cr11Ni stainless steel, Brooks [67] has observed that the weld solidified as primary austenite and exhibited the characteristic cellular solidification microstructure with the cell size on the order of 2-3 microns, While the GTA welding of the same material showed that the GTA weld solidified as primary δ with the cell size of 10-15 microns, then most of which transformed to austenite upon cooling through the (δ+γ) two-phase field (Fig.2.13).

2.4 The scope of this work

From the above review, we can see that the research of welding in microgravity is very important for future space exploration. Laser welding will play a important roll in future space construction and repairing. This is not only because it has so many advantages such as high speed, ease of control, no contact requirement, no X-ray hazard, but also because it is possible to pump the laser directly from solar energy in space.

In our experiment, a CW CO_2 laser beam will be used for welding of AISI316 stainless steel. A bead-on-plate laser welding will be conducted on 1.0mm thick stainless steel strips for welding experiments both on ground and in a microgravity environment. The microgravity environment will be obtained by parabolic flights of a KC-135 airplane which can provide both microgravity (10^{-2}g) and high gravity (1.8g) environment for about 20 seconds in each parabolic manoeuvre of the aircraft flight. Welded samples will then undergo metallurgical analysis with optical and scanning electron microscopy to determines the characteristics and the effects of low gravity environment.

CHAPTER 3

EXPERIMENTAL PROCEDURE

3.1 Materials and processing

1.0mm thick AISI 316 stainless steel strips, with Fe-17%Cr-12%Ni-2.5%Mo-1.5%Mn (wt%), were obtained by cold-rolling 1.5mm commercial AISI 316 stainless steel sheet, followed by shearing to proper size (10mm x 150mm) suitable for the laser welding sample holder. The rolling reduction reached nearly 33% in thickness after several passes. Each strip was then annealed at 1050^{o}C for 1 hour and water quenched to room temperature to release the residual stress and for grain recovery.

Generally, AISI 316 stainless steel has very good weldability compared with other stainless steels. In most of its applications it is easy to make sound welds without preheating and the weld can be put into service without heat treatment after welding while having properties closely comparable to those of the base metal.

3.2 Laser beam welding systems-LAMPS

A continuous wave(CW), carbon dioxide laser materials processing system(LAMPS) has been used in both ground-base tests(for optimizing the welding parameters) and microgravity tests. The CW CO_2 LAMPS, as shown in Fig.3.1, was developed by MPB Technology Inc.(Pointe Claire,Quebec) and the University of Waterloo. LAMPS consists of three parts. Part A is a control console which contains a computer. All the data

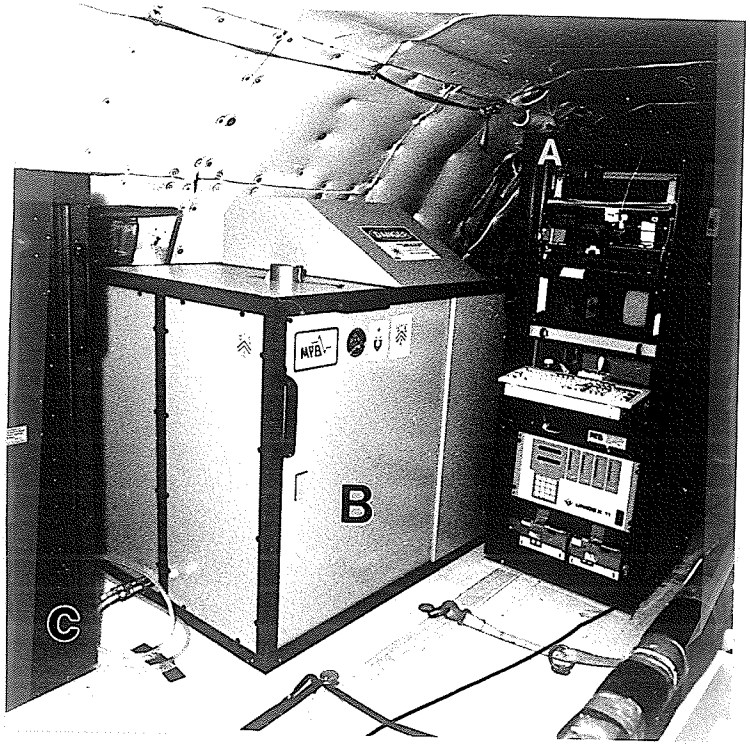

Fig.3.1 LAMPS on board KC-135.

a)Control console

b)Laser welding cabinet

c)Gas/Water supply

including acceleration data or gravity level, laser welding power, welding speed can be recorded for later analysis. The laser welding is performed inside part B which the exterior of the frame is fully covered with aluminum sheet for safety reasons. There is no control over the experiment except translation speed and power to the laser, once the box is closed. There have been no alignment problems either with the laser resonator cavity or the beam delivery system. Part C provides the cooling water to protect the laser head and welding shielding gas which is argon.

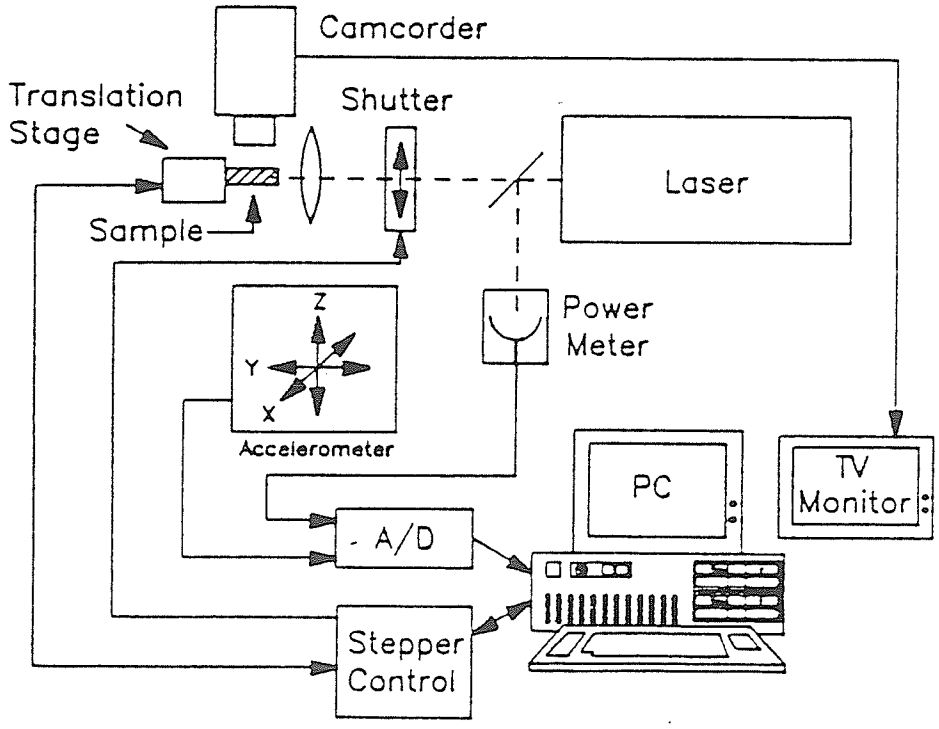

Fig.3.2 A schematic diagram of the apparatus.

Fig. 3.2 shows a schematic representation of the apparatus. Data on the time dependence of the gravity level was obtained using an accelerometer with 10^{-4}g accuracy along each of the three axes. The accelerometer was mounted to the laser test bed and monitored and recorded by the computer. The system was designed so that the welding can be initiated at preset micro- and hyper-gravity thresholds during parabolic flight and terminated after a specified time delay (usually 20 sec). Since parabolic orbits on the KC-135 typically provide 23 sec of low-g environment, adequate time was available for the establishment of equilibrium welding conditions.

The maximum power of LAMPS is 120 watts which is the maximum high power consumption for the KC-135 environment and it is supplied from the aircraft power bus. LAMPS was selected to be the welding source because it satisfied the weight and size limitations required by the KC-135. This kind of machine is ideal for welding thin and delicate components with little or no distortion of the surrounding metal due to its limited heat build up.

3.3 Ground base laser welding tests

Before conducting the microgravity welding tests, the LAMPS was first tried on the ground. Five process variables have been identified as important factors influencing the welding of AISI316 stainless steel strips. These are: laser power, traverse speed (welding speed), diameter of the focused beam, depth of focus and type of gas shielding.

The laser beam power was measured by a water cooled calorimeters. The laser beam was directed to the calorimeter by a mirror. In ground base laser welding experiment powers ranged from 90W to 120W have been used while the welding speeds were varied between 0.01cm/sec and 0.50cm/sec to provide a variety of welding conditions.

For efficiently welding 1.0mm thick stainless steel strips, a short focal lengths (<150mm) was used and the focal point was kept 0.1mm underneath the workpiece to achieve the maximum penetration.

Argon gas has been used as a shielding gas for both the ground base tests and KC-135 parabolic experiments. It gives some protection to the focusing optical components from deterioration resulting from fume and spatter due to the vulnerability of short focal length system to damage, and ensures effective transmission of the beam through the hot region of gas just above the workpiece, meanwhile protecting the molten material in the weld pool from reaction with the atmosphere.

A bead-on-plate laser welding was conducted both during the ground base tests and during the KC-135 parabolic flights. This gave enough welding information at the least expense by omitting joint preparation and seam-tracking requirements.

3.4 KC-135 parabolic flight experiments

In these experiments, LAMPS was used to make an autonomous weld bead in both low-g

and high-g environment. Therefore, the microgravity effect in space which will influence the quality of a weld was simulated. The equipment and human operators were flown on NASA's KC-135 in Houston Space Center, as it flies parabolic maneuvers to create low gravity as shown in Fig.3.3. Two gravity levels were obtained during one parabolic flight: high-g (1.8g) and low-g (10^{-2}g). The duration of each gravity level can last as long as 20 seconds. In total 12 parabolic flights were performed in each flight for laser welding experiments.

The power of laser beam used was 120 watts and it was kept constant during all the parabolic flights as shown in Fig.3.4. So was the translation speed which was kept at 0.06mm/sec. This means the laser beam welding were conducted continuously along with the variation of gravity levels.

The experiment is designed so that variations that will occur are directly attributable to the changes in g-level. So the only variable which changes in few seconds of g-transition is the g-level itself. Laser power, welding speed, focus, specimen conditions, environment temperature are all constant when g-level is abruptly reduced or increased.

3.5 Weld sample analysis

After completion of the laser welding, the welded specimen were shipped to the metallurgical laboratory in University of Manitoba. First, careful examination of the weld

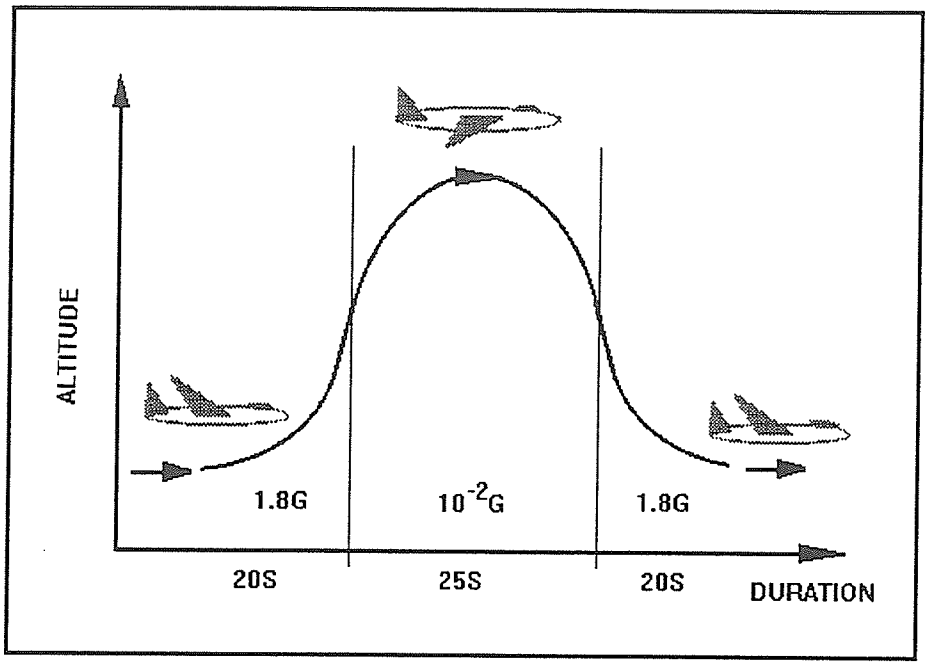

Fig.3.3 KC-135 aircraft flight trajectory.

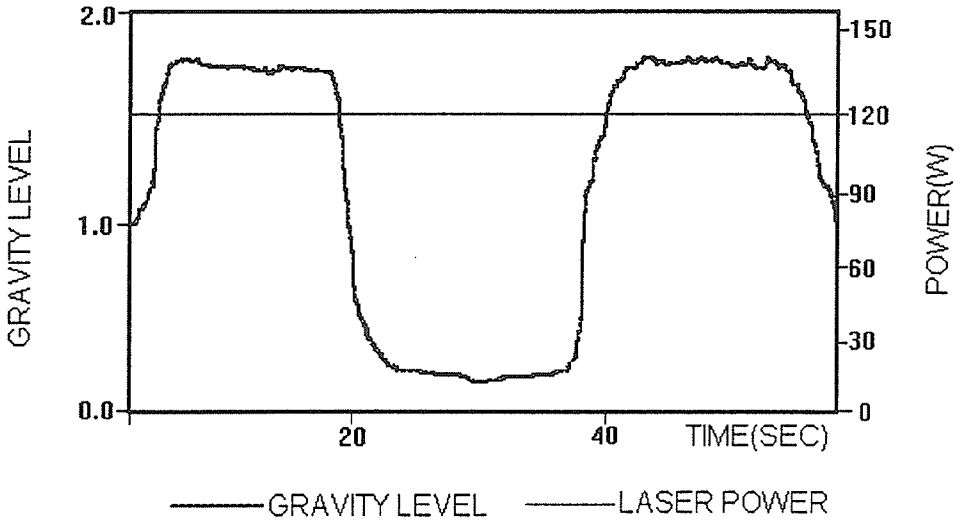

Fig.3.4 Gravity level and laser beam power.

surfaces was performed, and the welds were evaluated for suitability to be further tested. Specimens without irregularities that reduced viability for data collection were selected for detailed examination. Surface features of each selected weld were photographed by optical microscopy prior to sectioning.

The specimen were sectioned at both transverse and longitudinal cross sections as shown in Fig.3.5. Transverse sections revealed the weld pool shape in a plane normal to the translation axis. The longitudinal sections cut the weld bead vertically in the plane containing the translation axis and this could revealed the microstructural variations from front to back in the pool and, therefore, the convective patterns of the weld pool were clearly visible, so did the variations in partial penetration with position.

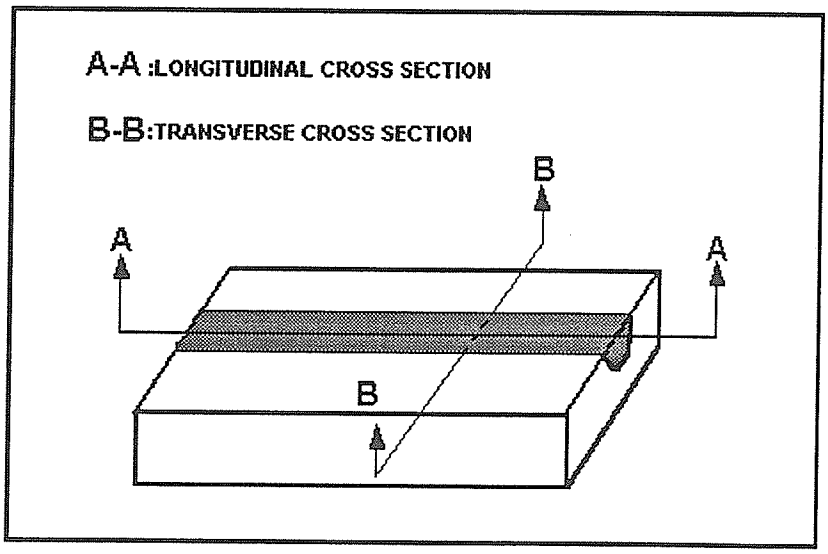

Fig.3.5 Sectioning position on welded sample for metallurgy analysis.

The specimens were then mounted in bakelit and polished to 1 micron diamond paste. The weld configuration and penetration were first observed by using the optical microscope. The weld microstructure analysis was performed by using a JXA-840 scanning electron microscope. An EDAX system was utilized for weld composition analysis. All the weld bead width and penetration were measured by optical microscope. For the purpose of weld surface observation, the oxide layer produced by the welding process was removed by chemical surface cleaning using a chemical solution (30ml HNO_3 + 4ml HF + 100ml water) for 1hr. at 40^0C. All cross-sections were electrolytically etched with 10% oxalic acid before observation.

CHAPTER 4

RESULTS AND DISCUSSION

4.1 Laser welding experiments--ground base tests

4.1.1 Effect of welding parameters on laser welding AISI316 stainless steel

Power and Speed

To establish the relationships between the laser beam welding parameters and weld bead geometry, a couple of bead-on-plate laser welding experiments were performed on 1.0mm thick cold-rolled AISI316 stainless steel strips for partial-penetration welding. The measurements of bead width and penetration are shown in Table 4.1, together with the laser welding power and speed. The laser beam power selected here ranged from 90W to 120W, which is most suitable for thin sample welding. The welding speed varied from 0.01cm/sec to 0.10cm/sec. Bead width and penetration are plotted as functions of welding speed and power in Fig.4.1 and 4.2, respectively. In the experimental ranges of welding speed and laser beam power, both weld bead width and penetration decreased with the welding speed under a constant laser beam power, or increased with welding power under a constant welding speed. These results are in consistent with reference [15].

Fig.4.3 is the illustration of this relationship, based on the data in Fig.4.2, between the laser welding penetration and welding speed under constant welding power. This L type of pattern indicates two main processes involved in laser welding of stainless steels:

Table 4.1 Laser welding parameters and the measurements of weld penetration and width.

(Ground based tests)

Sample No.	Power watt	Speed cm/s	Melt Depth	Weld width
SBG121	120	0.02	0.20mm	0.43mm
SBG122	120	0.04	0.07mm	0.40mm
SBG123	120	0.06	0.06mm	0.40mm
SBG124	120	0.10	0.07mm	0.35mm
SBG125	120	0.30	0.10mm	0.32mm
SBG111	110	0.01	0.20mm	0.43mm
SBG112	110	0.02	0.12mm	0.35mm
SBG113	110	0.05	0.06mm	0.32mm
SBG114	110	0.07	0.07mm	0.34mm
SBG115	110	0.10	0.08mm	0.30mm
SBG101	100	0.01	0.18mm	0.39mm
SBG102	100	0.02	0.08mm	0.30mm
SBG103	100	0.05	0.07mm	0.30mm
SBG104	100	0.07	0.07mm	0.31mm
SBG105	100	0.10	0.07mm	0.30mm
SBG091	90	0.01	0.14mm	0.34mm
SBG092	90	0.02	0.10mm	0.28mm
SBG093	90	0.05	0.06mm	0.30mm
SBG094	90	0.07	0.05mm	0.30mm
SBG095	90	0.10	0.06mm	0.28mm

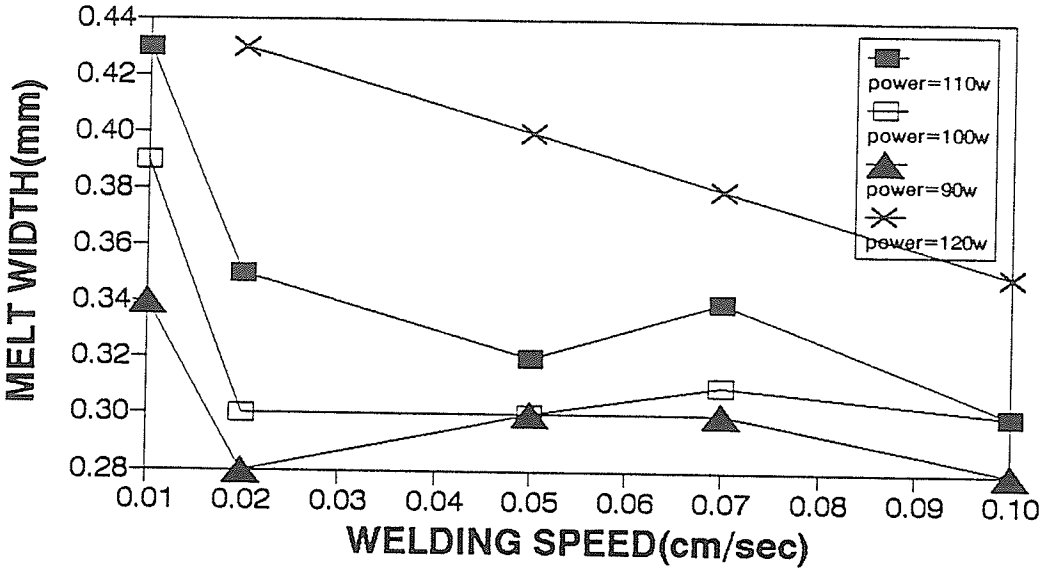

Fig.4.1 The relationship between the welding speed and weld width under constant welding power.

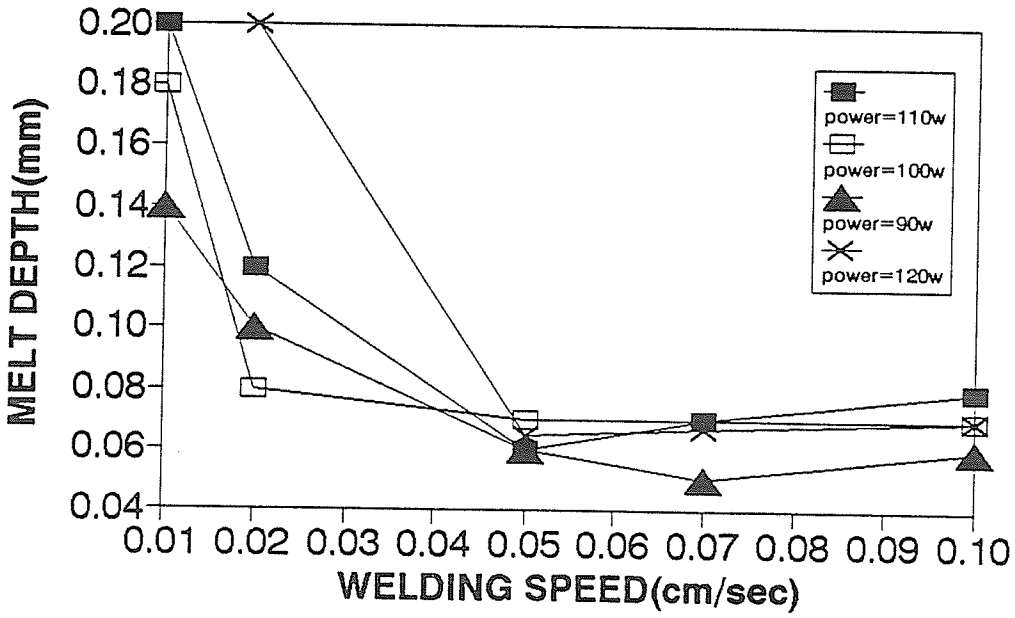

Fig.4.2 The relationship between the welding speed and weld penetration under the constant welding power.

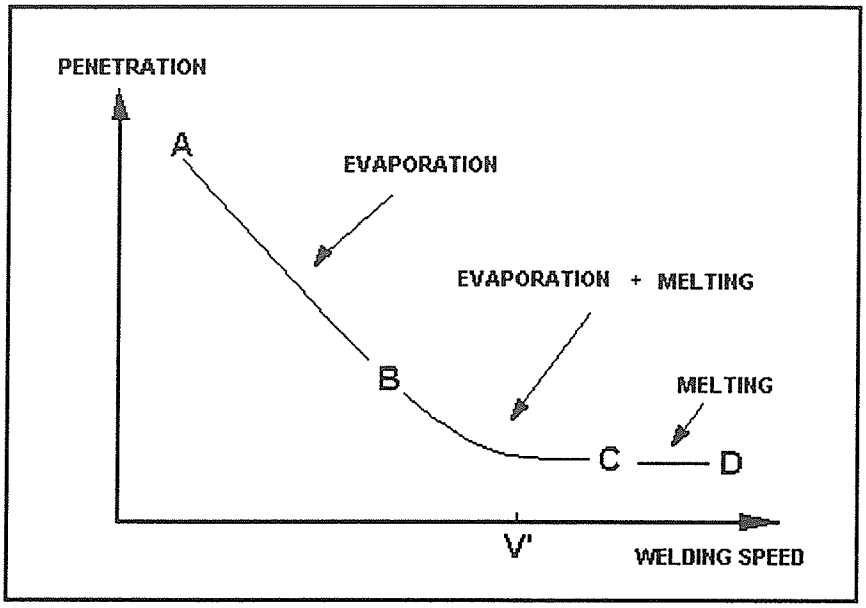

Fig.4.3 A schematic diagram of the relationship between the welding speed and weld penetration.

evaporation and melting. In range AB, the welding process is dominated by key-hole with a violent ejection of molten metals from the weld pool. In this part, slower the welding speed, more evaporation occurs which has been observed during the welding test, resulting in deeper penetration. This indicates that in this region of welding, the weld penetration is mostly contributed by weld metal evaporation. As an example, a cross section of a laser weld at power 120W and speed 0.01cm/sec has been shown in Fig.4.4(a). Instead of welding, it is actually a drilling process because most of the weld metal evaporates under this combination of welding parameters.

With the increase of welding speed, the heat input decreases and the temperature of the weld decreases to such an extent that, when welding speed reaches the threshold value-V',

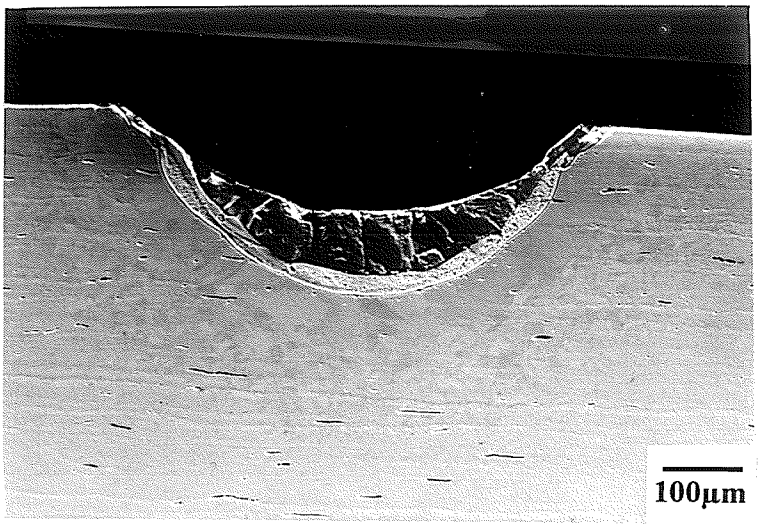

(a)

(b)

Fig.4.4 A cross section of laser beam welds at

(a) power=120W, speed=0.01cm/sec and (b) power=120W , speed=0.3cm/sec.

melting will play a dominant role in the welding process. Due to little evaporation, the weld attained a solidified bead as shown in Fig.4.4(b).

In the discussion of relationship between processing parameters and weld bead morphology, the heat input distribution from laser beam, heat conduction, convection in the molten pool and the base metal composition are all controlling factors. But the dominant factor to consider in laser welding is the heat input.

The heat input in laser welding can be defined as P/V as in reference [39], where P is the laser beam power at the workpiece and V is the welding speed. This parameter, which represents the energy deposited per unit length of weld, is usually correlated with weld penetration depth. It has been widely accepted as a parameter for collecting data on the laser welding of steels as a guideline for practical applications.

Fig.4.5 plots the weld penetration as a function of welding heat input. Over the range of heat input considered in this work, the relationship between weld penetration and heat input appear to be approximately linear. From this figure, it is clear that the increase of heat input will result in the increase of weld penetration.

Laser beam focussing

As mentioned in the last chapter, a short focal length has been used in the present laser welding experiment. Due to a reduced depth of focus, the focal point has to be adjusted

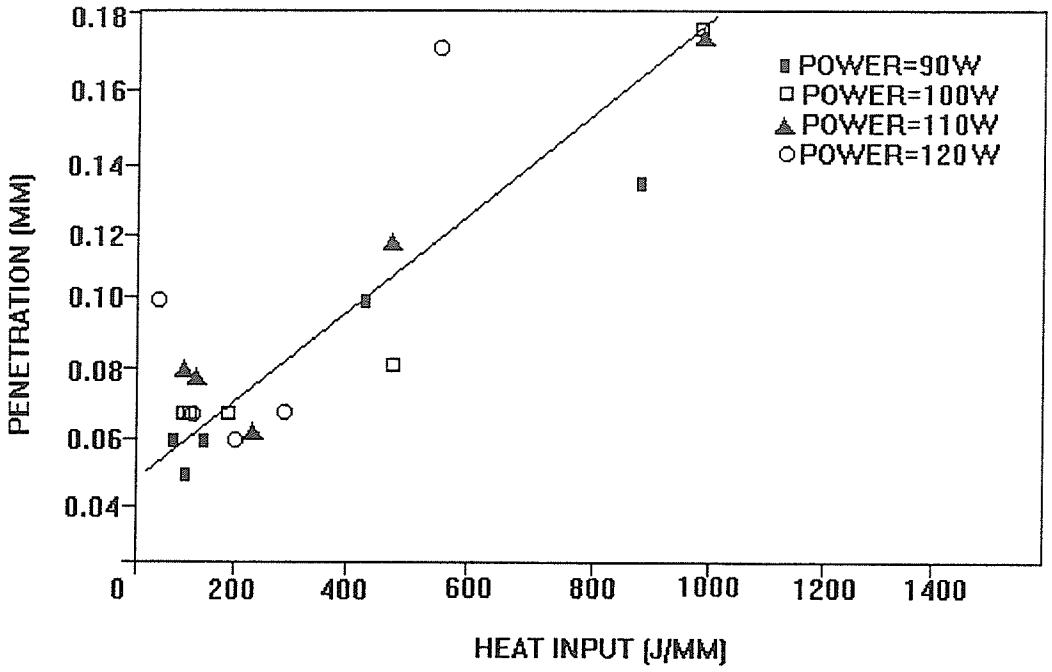

Fig.4.5 The relationship between heat input and weld penetration in ground based laser welding tests.

each time in welding 1.0mm stainless steel strips for achieving maximum penetration depth. From the experience of laser welding of steels, it has been learned that the optimum position for focal point is below the surface of workpiece. But the exact distance is dependent on the thickness of the workpiece and the laser power as well as the welding speed. For 1.0mm thick stainless steel strips in this work, the variation of penetration with the focal point is schematically illustrated in Fig.4.6. Here R is the effective range of focal position for the laser beam within which a good weld quality can be obtained. In our case R<=0.3mm and from our experience, maximum penetration can be achieved when the laser is focused 0.1mm beneath the workpiece top surface as

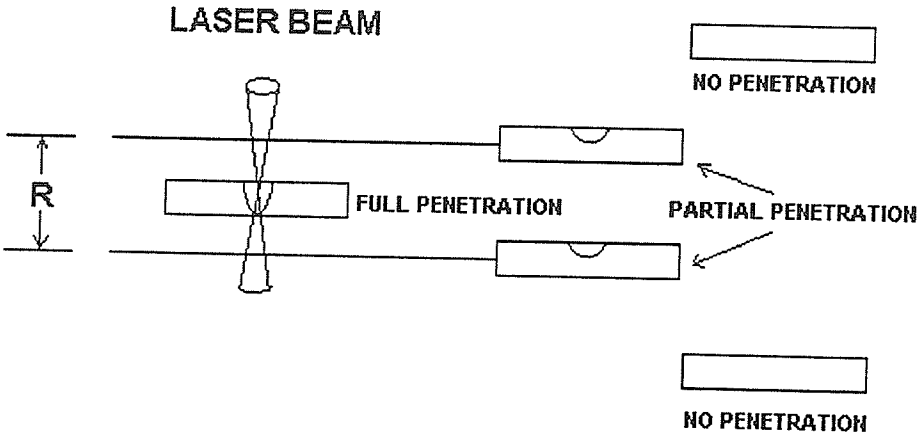

Fig.4.6 Focusing range of LAMPS.

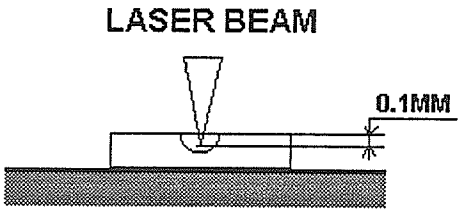

Fig.4.7 Focusing position in laser welding AISI316 stainless steel sample.

shown in Fig.4.7, when laser beam power is in the range of 90-120W. Generally, a higher focal position accuracy will be required when a lower output power is used. Therefore we selected to employ an output as high as possible in our work, to tolerate the variation of relative position between the laser beam and strip, because of the narrow range of R.

4.1.2 Microstructure of the laser weld

(1)Geometry of the weld fusion zone

Laser welding by LAMPS was performed under various conditions in ground base test. Fig.4.8 shows the surface appearance of a LAMPS welded AISI316 stainless steel. The

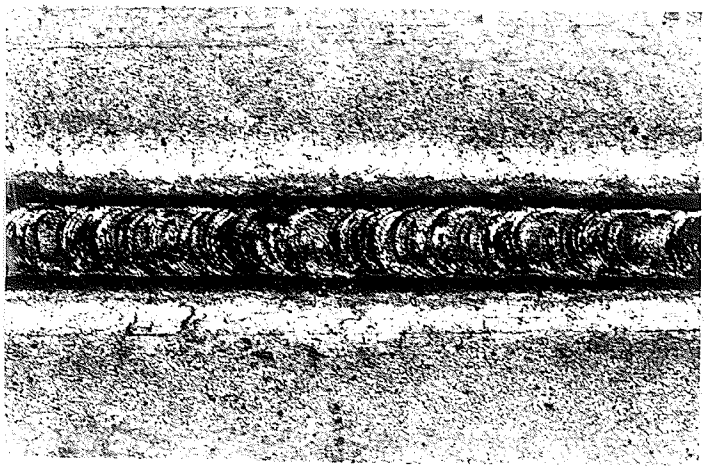

Fig.4.8 The surface appearance of a LAMPS welded AISI316 stainless steel on ground.

weld fusion zone geometry are as shown in Fig.4.4(a), (b) and Fig.4.10(a). Heat conduction melting mode of shallow penetration(Fig.4.4(b)) and key-hole(Fig.4.10(a)) mode of deep penetration were both observed depending upon the welding conditions. Based on the observation of many laser weld beads, their geometries were roughly classified into four types as shown in Fig.4.9. It appearers that type C and D are formed due to the spattering(evaporation) loss of the molten metal in weld pool. It has been found that any combination of laser welding power and welding speed that results in a higher heat input will likely result in a type C or D weld configuration compared with

those parameters with medium heat input. Only those of the medium heat input weld have a configuration like type B or A. Therefore higher heat input doesn't mean a sound weld configuration could be obtained, except the deeper penetration. To achieve a quality weld, using proper weld parameters is important.

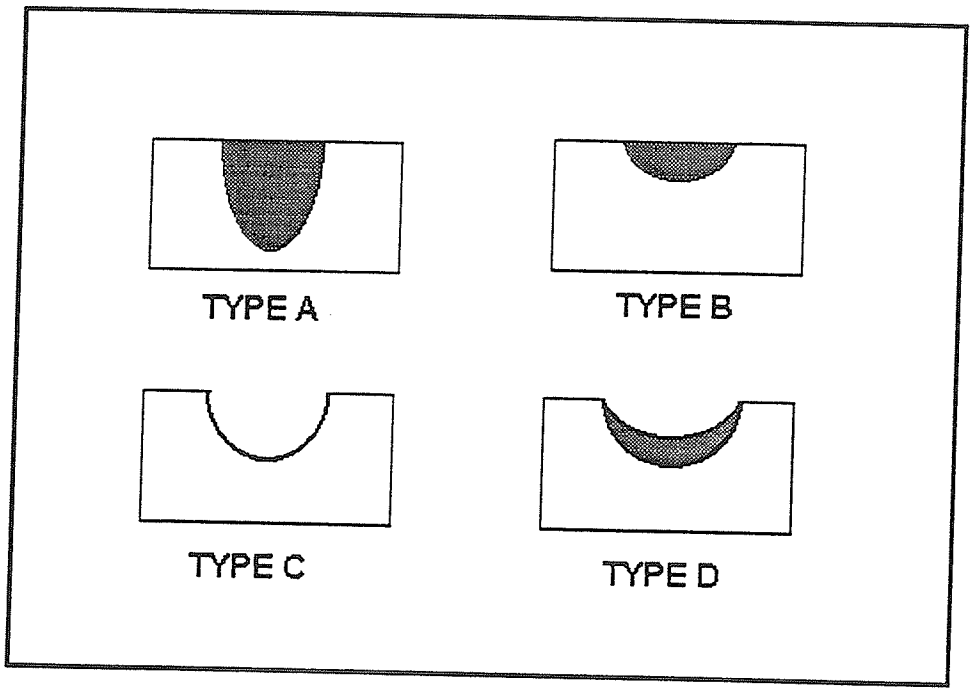

Fig.4.9 Laser weld geometries.

As mentioned above, type C or D weld is mainly due to the excessive intensity of laser beam acting onto the samples. With still higher heat input, there would be no weld metal left in the crater. This threshold value of the heat input that determines the characteristics of laser welding is controlled by material thermal properties.

Generally, the important properties of the material that affect the welding process include:

a) Reflectivity of the material surface and absorption coefficient of the material which directly affect the manner in which the laser beam is absorbed by the material;

b) Thermal conductivity and diffusivity. Those materials with a high thermal diffusivity accept and conduct thermal energy quickly. Since stainless steels have only 1/2 the thermal conductivity that of mild steels [35], it is very easy to accumulate the heat in weld pool and result in a D or C type weld during the laser welding. Therefore a medium heat input should be more suitable for laser welding stainless steels, compared with welding other metals, such as copper or aluminum.

c) Heat capacity and latent heat of the material. These properties decide the amount of energy required to cause the metal melting or evaporation. Due to the low value of heat capacity and latent heat, stainless steels requires less energy compared with mild steels. This means, it is very easy to cause a highly metal depleted weld condition during laser welding of stainless steels.

(2)Microstructure of laser beam weld

Fig.4.10(a) shows a transverse cross section of AISI316 stainless steel laser welded by LAMPS on ground at power=120W, speed=0.5cm/sec. It can be seen that when proper weld parameters are selected, sufficient penetration can be obtained without visible weld defects such as cracking and porosity.

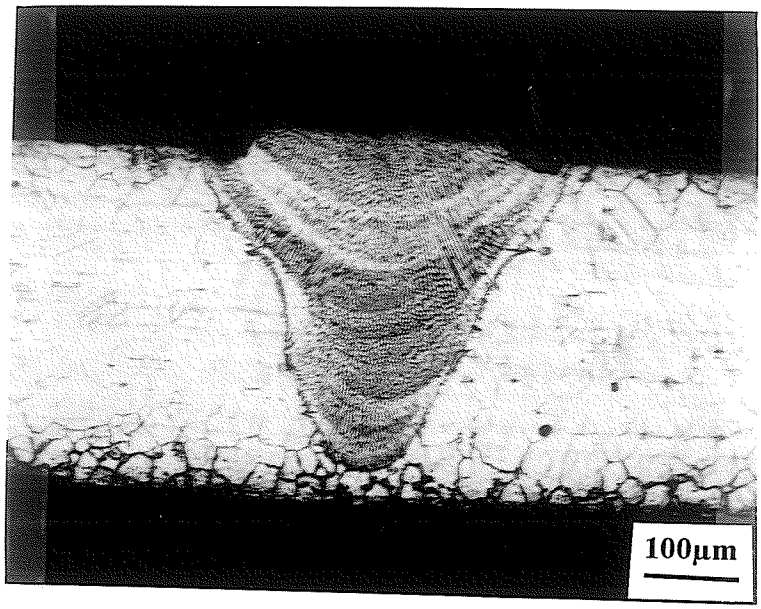

(a)

(b)

Fig.4.10 Transverse cross section of AISI316 stainless steel laser welded by LAMPS on ground at power=120W and speed=0.5cm/sec.

(a)optical micrograph of weld cross section,

(b)scanning electron micrograph at fusion boundary.

A dendritic microstructure is observed in weld fusion zone. No equiaxed grains can be identified as did in most of the conventional arc welding. This is in consistent with reference [65]. Those of grains in the upper-central part of the weld fusion zone are the cross sections of those dendritic grains grown along the welding direction. This may be due to the small size of laser weld pool and fast grains grow in the laser welding process. This solidification structure resulting from laser welding is of interest because of the extremely fine dendrite spacing exhibited. This is the direct consequence of the rapid solidification and the epitaxial influence of grain structure in the base metal on that in the weld metal. At higher magnification the dendrite pattern is more evident as shown in Fig.4.10(b). The epitaxy is also quite evident as observed at the fusion boundary.

Depending on the compositions investigated, laser weld microstructure of stainless steels can be categorized in three groups: fully austenite (γ); fully ferrite (δ); and duplex austenite plus ferrite ($\gamma+\delta$) [33]. Following conventional arc welding, the 316 alloy welds contain duplex ($\gamma+\delta$) microstructure and solidify in the primary ferrite mode [57, 60, 64]. For laser welding, however, the weld microstructure is also determined by welding environment, namely the cooling rates that the weld solidification undergo with. For certain laser power, 316 alloy weld microstructure could be duplex($\gamma+\delta$) at slow laser welding speeds or a fully austenitic microstructure could be observed at high welding speed [68]. Since the exact measurement of cooling rates in a laser weld pool is very difficult, we can only identify the weld microstructure by metallographic examination. Because a dendritic microstructure of 3-5 μm in spacing has been observed in weld fusion

zone near the fusion boundary as shown in Fig.4.11(a), we can suggest that the cooling rates during solidification are very fast (could be as fast as 10^5 ^{o}C/sec) [69] when welding at 90W with a speed of 0.30cm/sec by LAMPS. And in this case, 316 alloy weld would contain a fully austenitic microstructure and solidify in a primary austenitic mode. But for other welding with a relatively low speed, the cooling rate could be relatively slow, then a duplex (γ+δ) microstructure will still exist which solidify in a primary ferritic mode as shown in Fig.4.11(b), as observed in reference [58].

(3)Weld composition changes during laser welding of AISI316 stainless steel

During laser welding, an appreciable amount of alloying element vaporization takes place from the weld pool surface. As a result, the weld metal composition often differs significantly from that of the base metal. This problem is particularly pronounced when welding thin stainless steel strips.

Fig.4.12 is the x-ray mapping results of laser welds of 316 stainless steel which illustrates the effect of evaporation on the weld composition changes. Fig.4.12(a) is a video image of the weld obtained at power=120W, speed=0.01cm/sec. Due to its excessive heat input, significant amount of metal got depleted from the weld and formed a thick layer of weld slag above weld metal. X-ray maps Fig.4.12(b) gives an indication of the concentrations of alloying element chromium and nickel across the weld cross section at the same magnification as Fig.4.12(a) shown. On these images, the

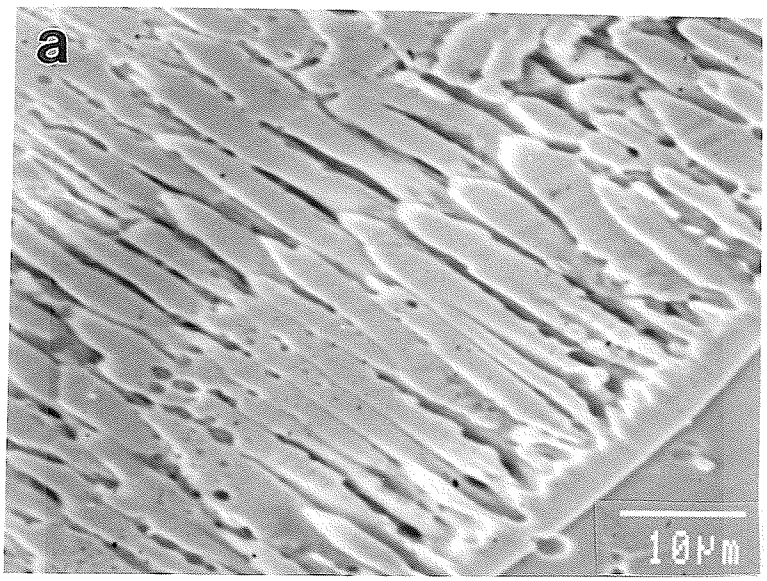

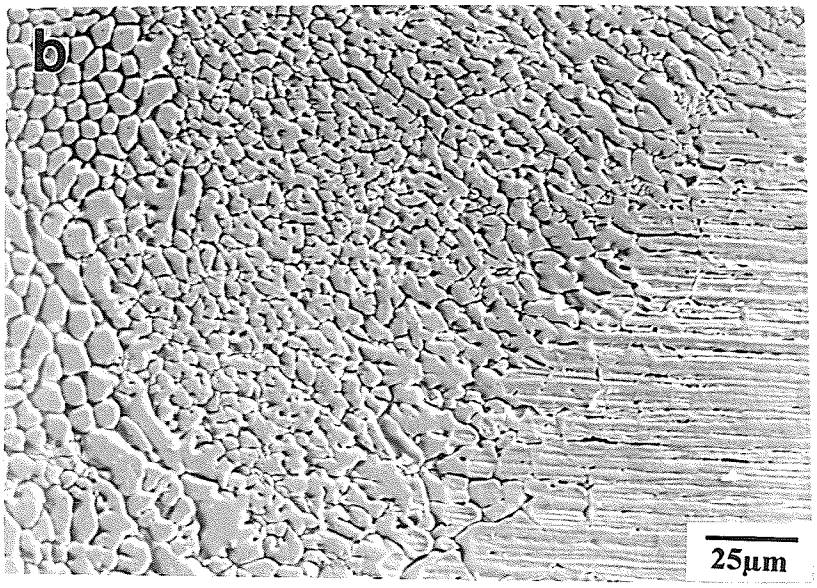

(b)

Fig.4.11 Scanning electron micrograph of laser weld fusion zone near fusion boundary.

(a)Power=90W, Speed=0.3cm/sec,

(b)Power=120W, Speed=0.1cm/sec.

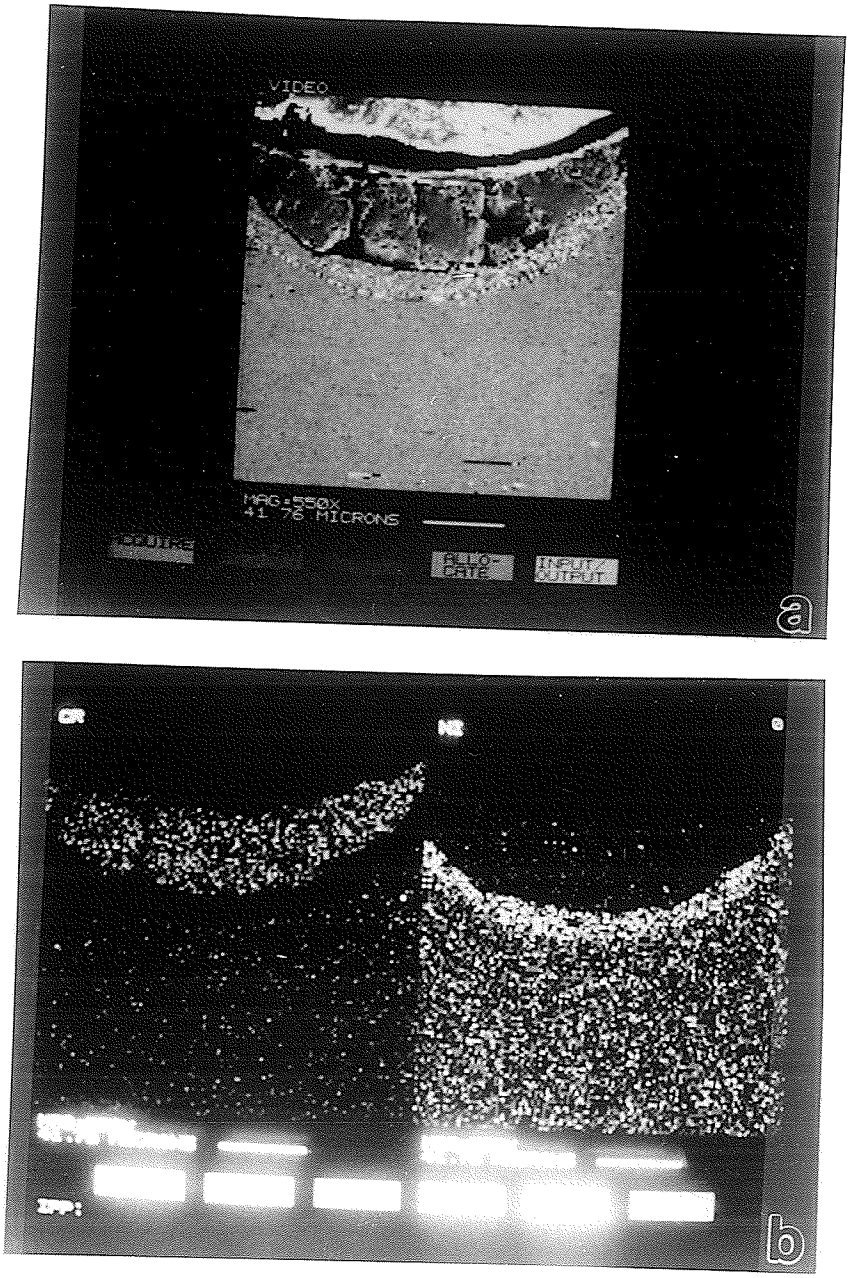

Fig.4.12 X-ray mapping of a stainless steel laser weld.

(Power=120W, Speed=0.01cm/sec)

(a)video image of the weld cross section,

(b)concentrations of chromium and nickel.

concentration of the element being considered is higher as the image is lighter. These results show that the weld is richer in nickel and poorer in chromium while the weld slag is richer in chromium, compared with base metal. This is because the chromium has higher vapour pressure comparing with nickel and it is more ease to evaporate under certain energy applied. Besides, chromium is actually a less noble metal than iron in the electro-chemical series, and thus the evaporated chromium gets oxidized at a very rapid rate to form the weld slag when the weld surface is exposed to oxygen.

4.2 Laser welding experiment aboard KC-135 parabolic flights

4.2.1 Weld macrostructure obtained in low and high gravity periods

As mentioned earlier, the KC-135 parabolic experiments by using LAMPS have been designed such that except for the gravitational level, all other parameters are kept constant during the parabolic flight. These parameters include laser power, welding speed, focus, specimen conditions etc.. Fig.4.13 shows a typical result of an AISI 316 stainless steel sample welded during the KC-135 parabolic flight. As laser travels along the stainless steel sample length, the weld bead goes through the low gravity level(10^{-2}g) and high gravity level (1.8g) periods for 12 times. The welds marked by a light point represent the welds when gravity level was reduced during the parabolic flight and rest of others are high gravity welds.

It is evident that a visible weld width variation occurred when gravity level changed.

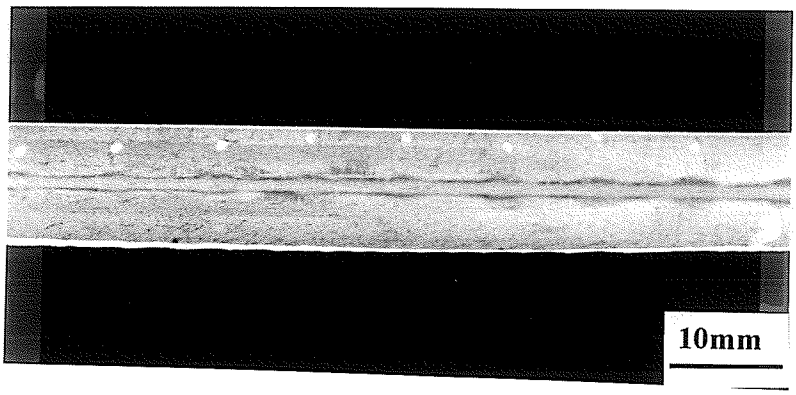

Fig.4.13 Optical micrograph of stainless steel 316 samples welded on KC-135 during parabolic flight. Light points indicate weld region when the gravity was reduced.

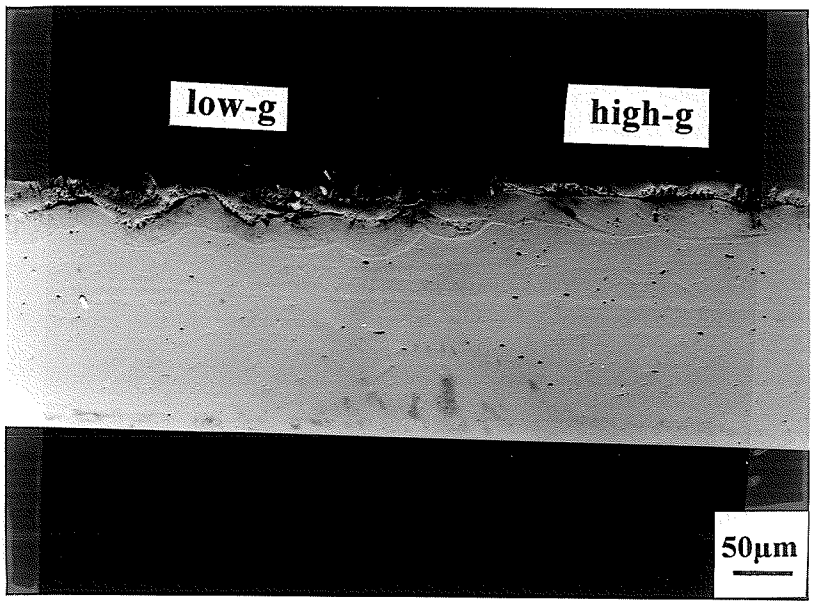

Fig.4.14 Optical micrograph of longitudinal section of stainless steel 316 sample welded during the varying gravity level, left is low-g and right is high-g.

Low-g welds exhibit a wider weld width with respect to high-g welds, and some oxidation also happened around low-g weld which indicates the argon gas shielding was not very efficient during the low-g welding periods, as shown in Fig.4.15.

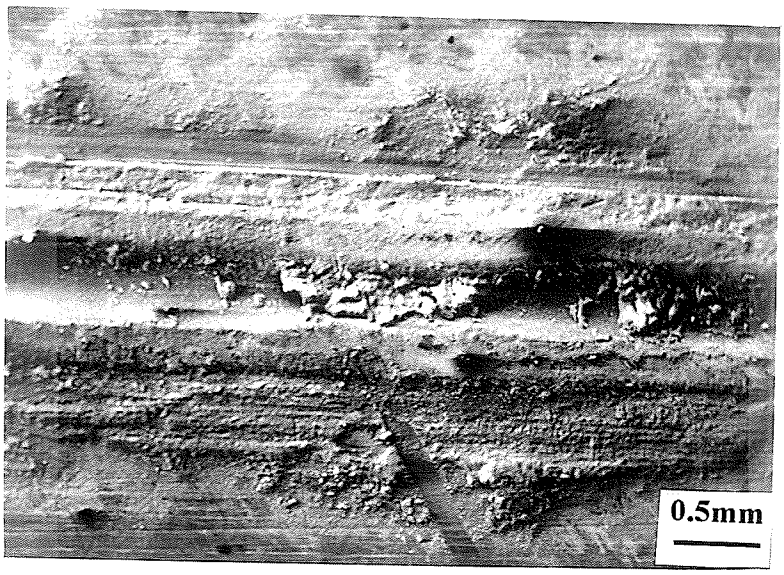

Fig.4.15 The surface appearance of a low-g weld showing the oxidation around the weld due to insufficient shielding of argon gas.

After the examination of the longitudinal cross section of this sample, the gravity level effects on the welding process are more clear, as shown in Fig.4.16. Measuring by an optical microscope, it was found that the average melt depth (weld penetration) is of the order of 0.08mm during the high gravity periods. When gravity level decreased to 10^{-2}g, the weld penetration is visibly deeper. The average melt depth of low-g weld increased by 62%, to the order of 0.13mm. This is different from the early research results[1] in which the penetration depth was found not affected by the absence of gravity, but it agreed, to some extent, with the results reported by references [4] and [5].

It is observed that the evaporation of the sample metal also occurred both in low-g and high-g period; the evaporation, however, was more pronounced in low-g period as shown in Figure 4.15. It is easy to see that although the total weld penetration increased, the thickness of the melted layer is almost constant. This indicates that significant amount of metal has been evaporated away during the low-g period.

4.2.2 Energy distribution analysis

In an attempt to explain the weld penetration changes during the parabolic flight experiment, The laser beam energy distribution at the beam-material interaction point as shown in Fig.4.16 must be analyzed. Here E_b is the incident energy coming from the laser source, E_p is the energy absorbed by the plasma and E_r is the part of laser radiation reflected by the sample surface and E_s is the energy absorbed by sample which will provide the energy for melting the metal.

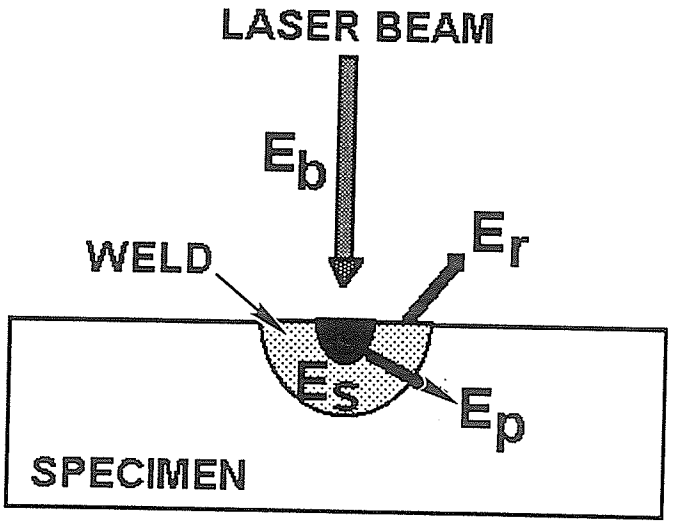

Fig.4.16 Schematic of energy distribution at beam-material interaction point.

In the simple analytical treatment of the laser-material interaction, the energy balance at the beam-material interaction point may be expressed as:

$$E_b = E_p + E_r + E_s$$

It is reasonable to assume that E_b and E_r were constant during the parabolic flight. E_p, however, is associated with the plasma compositions and intensity.

The formation of a beam-absorbing plasma at the beam-material interaction point is an important phenomenon in the laser welding [19-21]. The higher the intensity of the plasma, the more pronounced is the absorbing effect [21]. The energy absorption within the plasma can exceed 50% of the incoming laser energy [22]. In the present case, the plasma is mostly comprised of thermally ionized argon ions and metal vapours. Therefore, less Argon ions will reduce the intensity of the plasma and eventually reduce the E_p.

The observation of deeper penetration in low-g period leads to the conclusion that the energy absorbed by the sample may have increased when gravity was reduced. In order to keep the energy balance described in the above equation, E_p must have decreased. This indicates that the intensity of the plasma must have decreased in the low-g period. This decrease in plasma intensity can be explained in terms of a change in the shape of the Argon gas flow during the parabolic flight as shown in Fig.4.17.

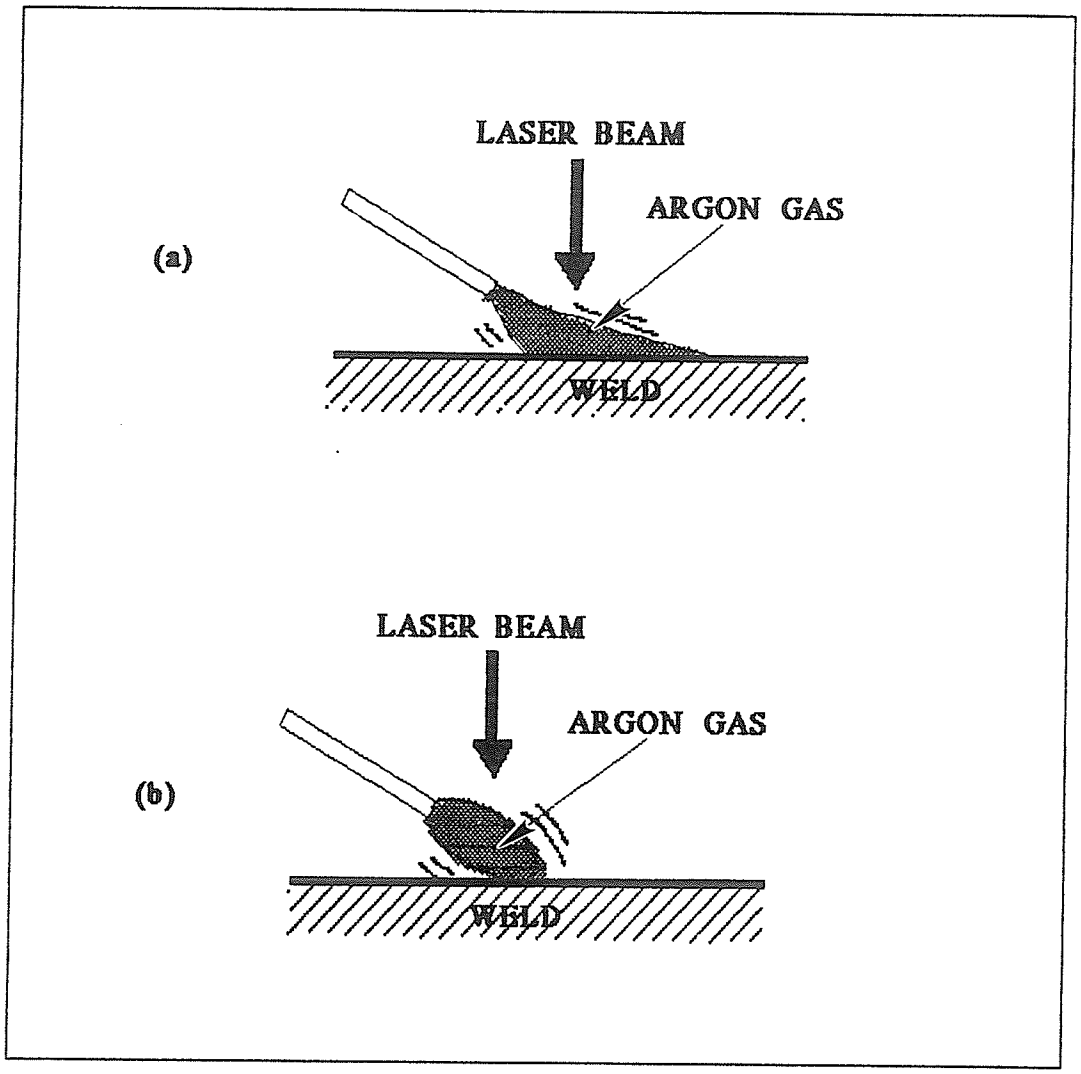

Fig.4.17 Schematic diagram showing shielding gas flow in high-g (a) and low-g (b).

Since the Argon gas is heavier than air, a tightly defined Argon gas flow(such as the one occurred in ground base test)will provide an effective shield to protect the weld from oxidation in high-g period as shown in Fig.4.17(a). At the same time, however, the Argon also leads to a high intensity plasma at the beam-material interaction point by providing easily ignited Argon ions, which will have a deleterious effect on the weld penetration [23], resulting in a shallow weld depth in high-g period.

In the reduced gravity period, however, a more diffused and stagnant Argon flow will most likely emerge as shown in Fig.4.17(b), resulting in a reduced plasma density at the beam-material interaction point which will reduce E_p, the energy absorbed by plasma. Therefore, the energy absorbed by the sample, E_s, will increase and lead to more volume of metal to be melted. Thus, a deeper penetration is produced in low-g period. At the same time, the less effective shielding will give rise to more oxidation around the weld during the low-g, as observed in Figure 4.14. This will also raise the coupling of the laser energy into the metal [24]. But this effect is expected to be small.

The increase of E_s during the low-g period will not only contribute to the penetration increase but also to the evaporation of molten metal as observed in Figure 4.14. This is attributed to the characteristics of low thermal conductivity of stainless steel which cause the temperature of molten pool to easily rise over the boiling point under the radiation of the laser beam.

4.2.3 Porosity in low-g welding

Existence of porosity in the welds has been reported in the early microgravity welding experiments [1]. In our samples welded during the KC-135 parabolic flights, porosity is also evident when gravity decreased as observed from the top surface of the weld in Figure 4.18. This shows very clearly how the extent of porosity changed as the gravity level changed. This is consistent with the previous results [26]. We can similarly consider that the removal of the porosity, formed during the welding process, became difficult upon entering a low-g period, and some gas bubbles even flowed into the molten pool because of the reduced buoyancy.

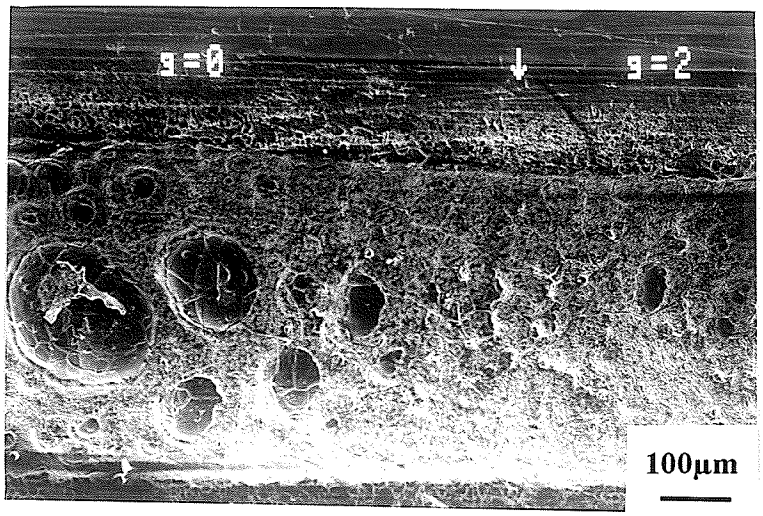

Fig.4.18 Scanning electron micrograph shows the comparison of the porosity on the weld surface along the changing gravity level.

4.2.4 Microstructure and compositions of low-g and high-g weld

Fig.4.19 shows the microstructure of laser beam weld obtained from KC-135 parabolic flight. Fig.4.19(a) is the longitudinal section of the weld obtained in high gravity period which is quite like the weld obtained in ground base test. Fig.4.19(b) and (c) are the welds in low-g periods. By comparing low-g and high-g weld microstructure, it is revealed that there are a lot of metal particles floating in the weld slag in the low-g weld as shown in Fig.4.19(b) and the low-g weld contains an extensive amount of defects (Fig.4.19(c)). The backscattered electron image of low-g weld shows that these defects (phase b in Fig.4.19(d)) are inclusions.

As shown in table 4.2, those inclusions b contains similar composition as slag c. Therefore, it is reasonable to assume that those inclusions are entrapped slag. In general laser welding process, the weld pool is usually driven by two kinds of forces: surface tension and buoyancy force. The convective mixing effect of these forces helps remove of slag from weld pool. But When the gravity is reduced or absent, the major driving force in the weld pool is the surface tension. In the case of laser beam welding, a high intensity source creates a small volume of weld pool, and the melting and solidification of weld metal happen rapidly. This only driving force may not work effectively and long enough to remove the slag. This may be the reason why the dispersed and entrapped slag in low-g weld is observed. And also due to the absence of buoyancy, the metal particles got suspended in the slag layer.

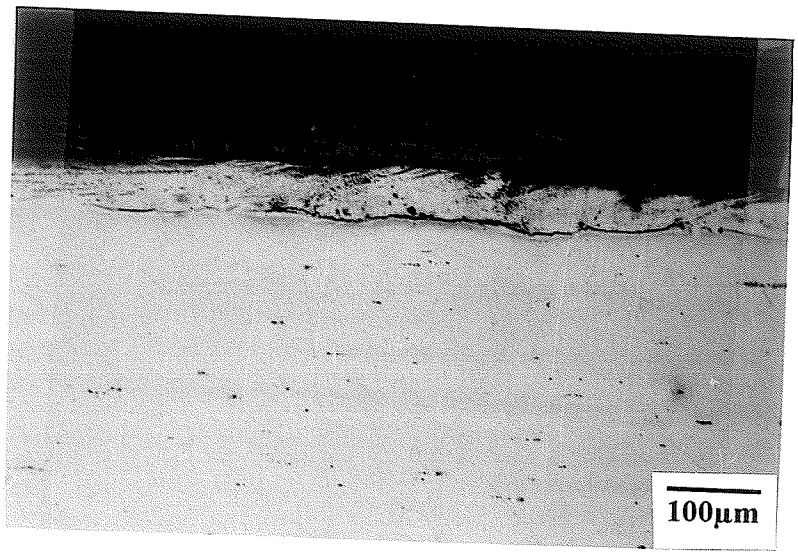

(a)

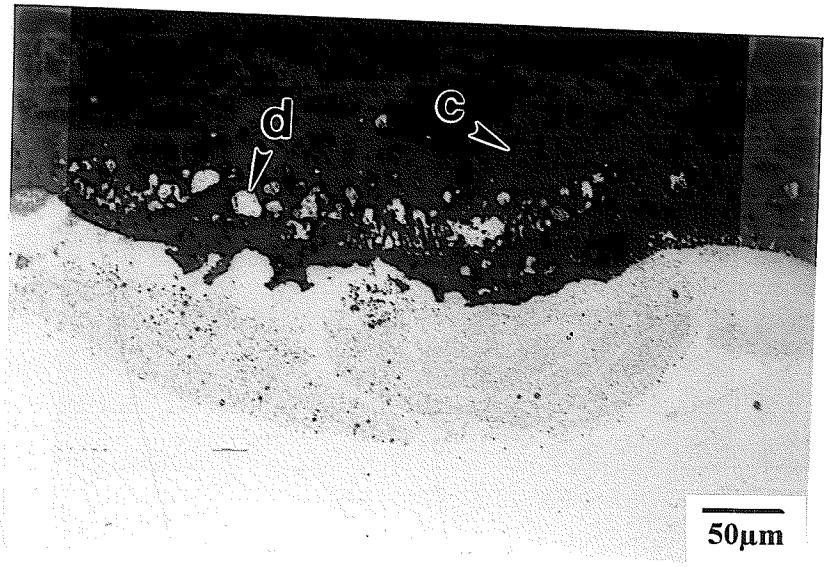

(b)

Fig.4.19 (a)Optical micrograph of the weld longitudinal section microstructure obtained in high gravity. (b)Optical micrograph of the weld longitudinal section microstructure, obtained in reduced gravity(no etching).

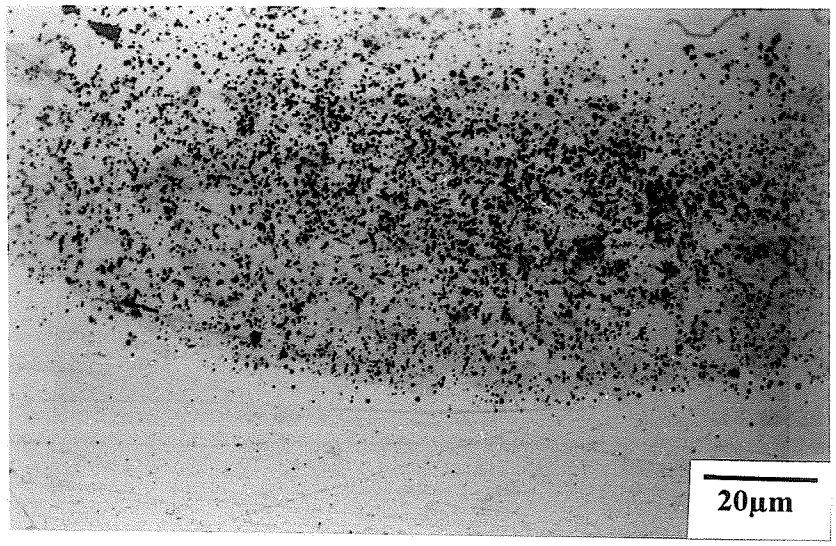

(c)

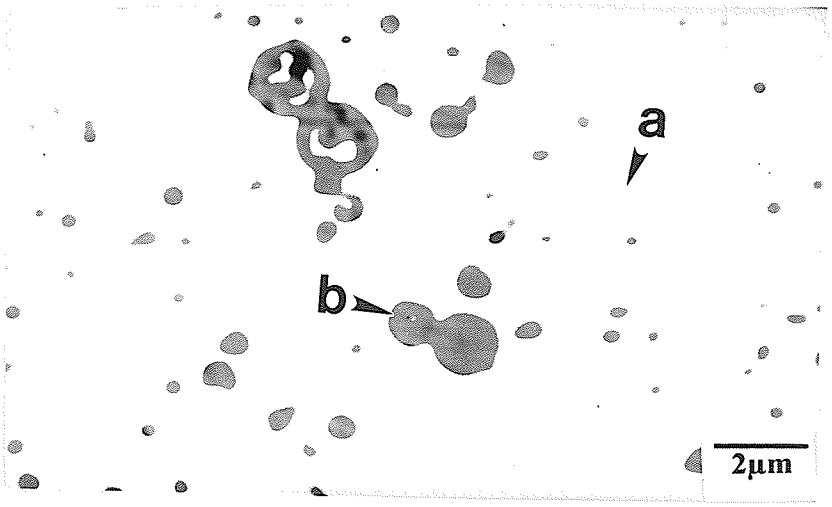

(d)

Fig.4.19(c)Same as (b) but at higher magnification showing low-g weld containing extensive amount of defects(no etching). (d)Scanning micrograph of low-g weld showing the defects are entrapped slag and porosity in the weld(no etching).

Table 4.2 The nominal composition of 316 stainless steel and the low-g weld composition

The nominal composition of 316 stainless steel in weight percentage

Fe	Cr	Ni	Mo	C	Mn
balance	17.00	12.00	2.5	0.08	1.5

The composition in low-g weld (w%)

Phase	Fe	Cr	Ni	Mo
a	78.71	0.39	19.22	1.69
b	51.12	44.95	2.29	1.63
c	41.30	57.00	0.56	1.14
d	86.48	9.21	9.21	1.85

The average compositions in both low-g and high-g welds are shown in Fig.4.20. The x-ray mapping of the low-g weld is shown in Fig.4.21. It is observed that the welds obtained both in low-g and high-g periods have a pronounced decrease in the concentration of chromium compared with base metal. The weld mainly consisted of iron and nickel which has austenitic microstructure. The changes in concentrations of iron and nickel along the weld as function of gravitation are evident. From high-g to low-g the weld concentrations are increased in iron by approximately 9% and decreased in nickel by approximately 25%. The concentration of chromium did not change significantly with the gravitation but maintained only a small weight percentage at around 0.3%.

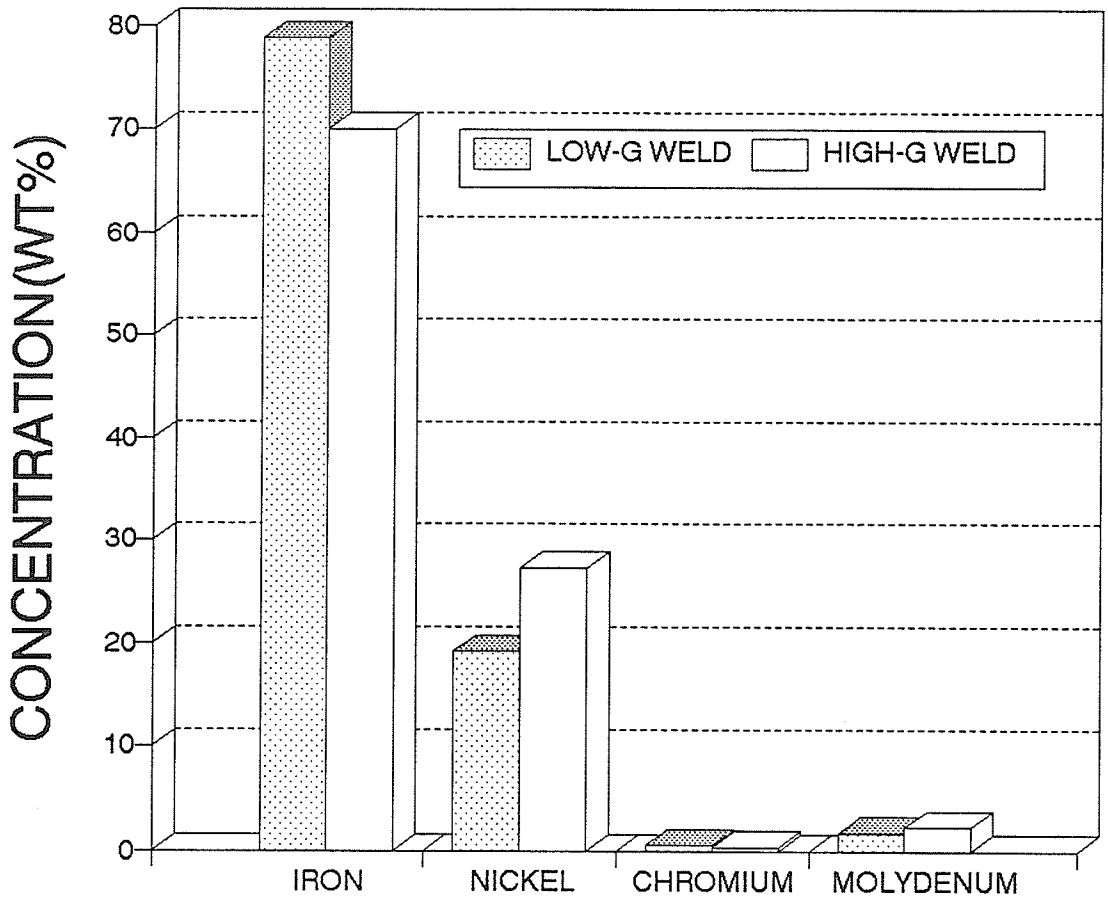

Fig.4.20 The average compositions both in low-g and high-g weld.

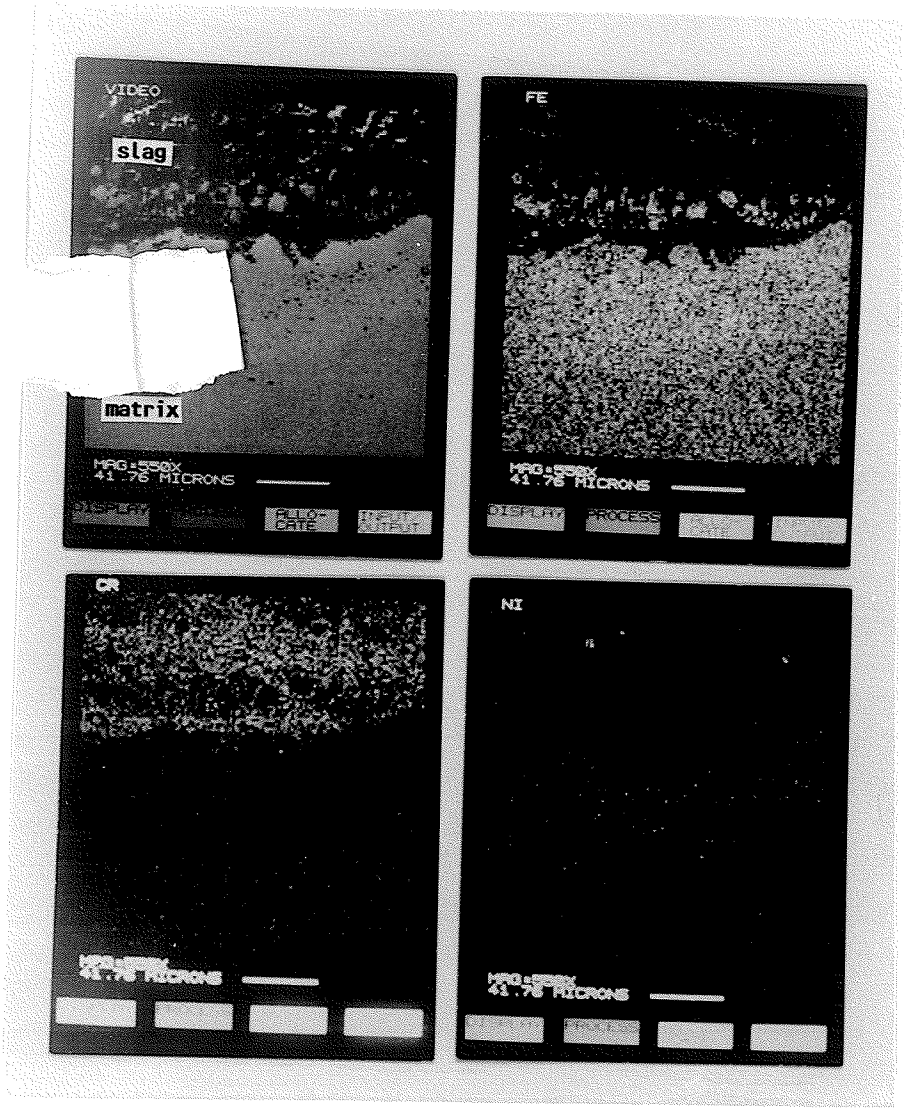

Fig.4.21 X-ray mapping of low-g weld.

The molybdenum almost has the same value as the base metal and no concentration changes is observed.

4.2.5 Weld pool behaviour in changed gravity environment

We have discussed the plasma effect in the analysis of low-g weld geometry changes due to the variation of gravity level. But the weld shape is also related with the fluid flow in weld pool during the welding process. The consideration of weld pool behaviour in reduced gravity environment may offer more explanation for understanding the microstructure of low-g weld..

However, it is difficult to exactly explain the low-g weld pool behaviour, because the development of a weld pool is influenced by the simultaneous occurrence of several important physical processes. These include: the amount of heat transferred from the laser beam to the workpiece, the fluid flow in the weld pool, and the accompanying convective heat transfer.

Previous work by several investigators [65, 69, 70-72] has shown that the coefficient of the surface tension, $d\gamma/dT$, where γ is the surface tension of the solution at the temperature T, is the critical variable that significantly influences and often controls the fluid flow in the weld pool.

For most of metal and alloys $d\gamma/dT$ is negative. Thus, the surface tension is highest near

the solid-liquid interface(where the temperature is lower) and causes the flow to be outward and away from the centre of the pool as shown in Fig.4.22(a). Only when surface active elements, such as sulphur or oxygen is added into the pool, a positive $d\gamma/dT$ can be produced, resulting in a higher surface tension at the centre of the pool, causing an inward flow as shown in Fig.4.22(b).

During the laser beam welding of AISI316 stainless steel, the driving forces for convection in the weld pool are surface tension and buoyancy. The convective mixing effects of these forces help remove slag from the weld pool. Due to high surface temperatures, the coefficient of the surface tension $d\gamma/dT$ is largely negative, causing a radially outward flow at the weld pool surface. And this flow is augmented by the buoyancy driven flow in the interior of the pool. In the absence of any significant opposing forces, the resulting fluid pattern would be same as shown in Fig.4.22(a). This radially outward flow produces a relatively shallow weld pool by transferring the heat from the centre to the periphery, as observed in Fig.4.23, which is obtained in a ground base test.

However, when the buoyancy force is reduced or absent as in the KC-135 parabolic flight experiments, the major driving force in the weld pool is surface tension. Because of the small weld pool size and rapid melting and solidification process in laser welding, this driving force alone may not work effectively and long enough to maintain the radially outward fluid flow in low-g weld pool. On the contrary, a downward flow at the centre

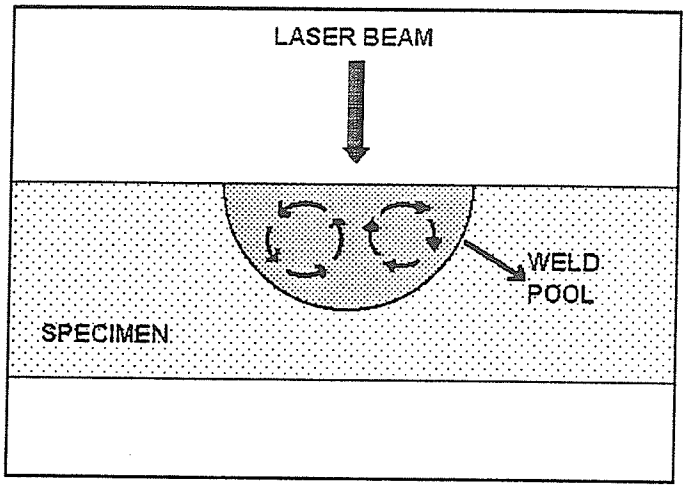

(a)

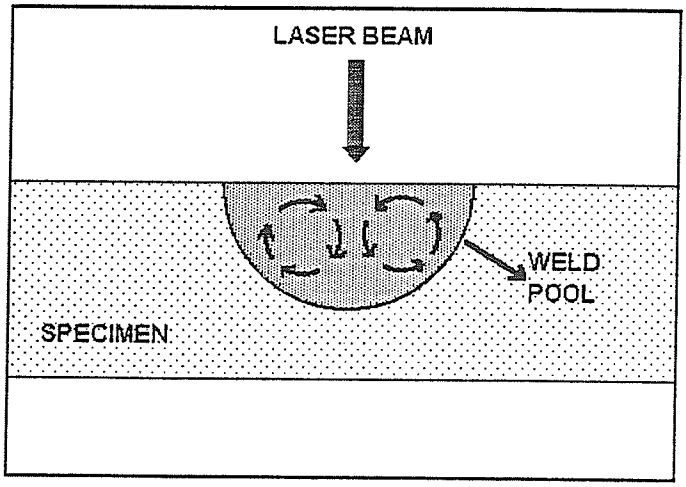

(b)

Fig.4.22 Schematic diagram of weld pool fluid flow pattern

(a)outward and (b) inward.

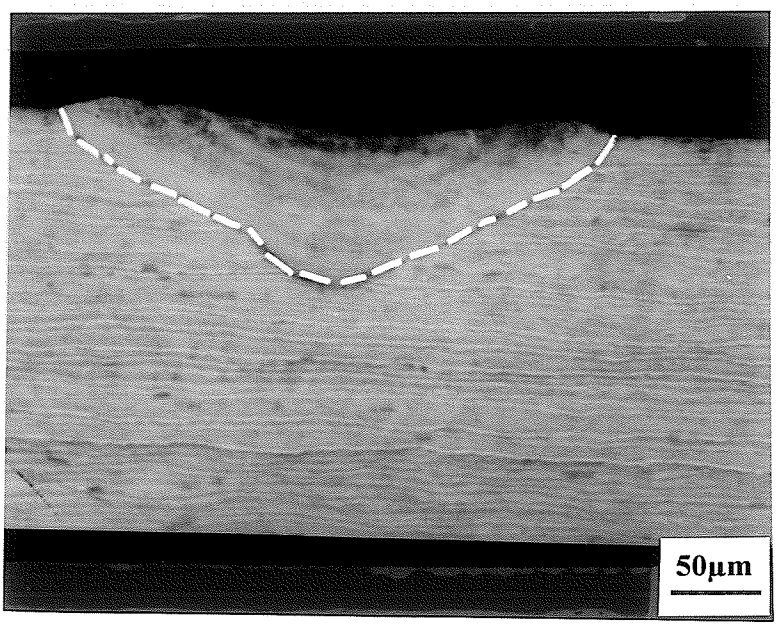

Fig.4.23 A cross section of laser weld. Power=90W, Speed=0.10cm/sec.

of the pool could be produced due to the absence of buoyancy, and such a flow would transport hot liquid melt at the centre of the weld pool from the surface to the bottom, causing increased depth of penetration during the low gravity welding period as observed in Fig.4.14.

4.2.6 Future work

The results presented in this study have shown the influences of gravity level on laser welding process. The change in weld geometry and microstructure with the variation of gravity levels have been considered as a result of unstable gas shielding and possibly a change in weld fluid flow pattern during the welding process. In future work, it would be more appreciated if the shielding gas movement, weld pool fluid flow could be visually

recorded for better understanding of the gravity effects. Therefore, an organic material, such as succinonitrile which is often used to model metals in solidification studies, is suggested to be used in microgravity laser welding, because it is transparent so by using optical camera the weld fluid behaviour during the melting and solidification could be recorded for later analysis.

Due to the high expenses involved in this experiment, the access to KC-135 parabolic flight is quite limited. To date, we still need more trials to make conclusive comments on the effects of gravity on weld solidification, such as the weld segregation, grain grow pattern. However, it will be worth to try TIG welding on ground by different welding position such as vertical, overhead (Fig.4.24) to compare them with flat welding and investigate if the gravity causes any difference or to what extent on weld solidification. During the literature review we haven't found the systematic study on this topic. By doing so, the direction of gravitational force can be varied, even though the absence of gravitational force is impossible to be simulated in this way. TIG welding on ground to study the gravity effect will be an economical addition for microgravity welding study, and meanwhile, it has some industrial application value.

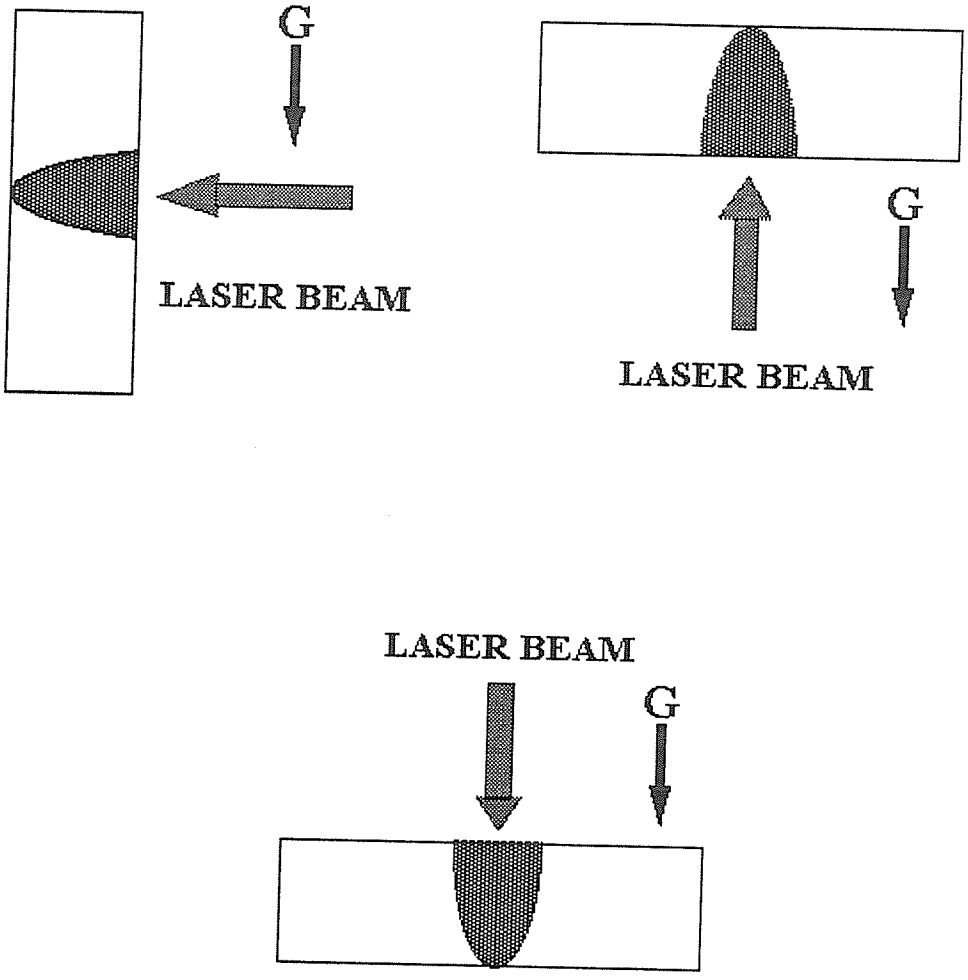

Fig.4.24 TIG welding positions on ground.

CHAPTER 5

CONCLUSIONS

1.LAMPS welding on thin AISI316 stainless steel strips resulted in welds that could meet the partial penetration requirement with no defects such as cracking, porosity.

2. The welds made with the slower welding speed or higher welding power showed an increase in evaporation (ejection) of weld metal and resulted in a deeper penetration with cater. The composition analysis showed that the weld slag is rich in chromium and the weld metal rich in nickel.

3. The KC-135 parabolic flight experiments have shown that the changes of gravity level have an effect on the argon protected laser welding of stainless steel. In our experiment, wider welds with deeper penetration are observed in low-gravity periods. Those changes have been considered as the results of unstable status of shielding gas, which results in the redistribution of incident laser energy.

4. It has also been observed that the low-g welds lose more alloying elements compared with the high-g welds. The microstructure of a low-g weld is characterised by a dispersed and entrapped slag. Porosity is observed when gravity is decreased. Weld metal particles have been found floating in the weld slag.

5. From these experimental results, it is suggested that low gravity gas protected laser beam welding will face more challenges than ground base welding.

REFERENCES:

1. J. K. Watson, D. W. Dickinson and S. I. Rokhlin; Survey of Soviet space welding technology development, Proceedings of space'88, New Mexico, USA, Aug. 29-31, 1988.

2. B. Irving; Electron beam welding, Soviet style: a front runner for space, Welding Journal, pp.55-59, July 1991.

3. "News of the industry", Welding Journal, p68, Dec. 1991.

4. W. F. Kaukler, etc.; Laser welding in space, TWR'89, Tennessee, USA, May, 1989.

5. G. L. Workman and W. F. Kaukler; Laser welding in reduced gravity, Proceedings of the laser materials processing - ICALEO'90, p430-440, 1990.

6. D. W. Dickinson, etc.; New advances for welding in unusual environments, Proceedings of new advance in welding and allied processes, Beijing, China, May 1991.

7. K. N. Tandon and G. Wang; Report to MPB's Technology Inc., University of Manitoba, Dec. 1991.

8. R. K. Holbert, T. M. Mustaleski: Laser welding of thin austenitic stainless steel sheet, Proceedings of the conference on the laser vs the electron beam in welding, cutting , and surface treatment, 1985, pp315-323.

9. T. M. Weedon: Application of solid state lasers in manufacturing industry, ICALEO'82, pp1-11, 1982

10. J. T. Luxon, D.E. Parker and P.D. Plotkowski; Laser in manufacturing-an introduction to the technology, IFS(Publications) Ltd. and Springer-Verlag, Berlin, p46. 1987.

11. B. Petesch, M. Robin; Laser welding of thin nickel sheets, ICALEO'86, pp145-155,

1986.

12. J. E. Anderson and J. E. Jackson; Theory and application of pulsed laser welding, Welding Journal, pp.1018-1026, Dec. 1965.

13. R. H. Fairbanks, Sr. and C. M. Adams, Jr.; Laser beam fusion welding, Welding Journal, pp. 97s-102s, March 1964.

14. W. N. Platte and J. F. Smith; Laser techniques for metals joining, Welding Journal, pp.480s-489s, Nov. 1963.

15. ASM Metal handbook, Vol. 6, p656, 1983.

16. S. Katayama, C. D. Lundin, J. C. Danko and T. D. Mckay; Laser weldability of aluminum alloys, TWR'89, 1989.

17. M. M. Schwartz; Modern metal joining techniques, John Wiley & Sons, Inc., 1969.

18. E. A. Metzbower; Laser beam welding: thermal profiles and HAZ hardness, TWR'89, 1989.

19. M. C. Fowler and D. C. Smith; Ignition and maintenance of subsonic plasma waves in atmospheric pressure air by CW CO_2 laser radiation and their effect on laser beam propagation, Journal of applied physics, Vol 46, pp.138-150, 1975.

20. E. Sturmer and M. Von Allmen; Journal of Applied Physics, Vol. 49, p.5648, 1978.

21. A. Matsunawa; Physical phenomena and their interpretation in laser materials processing, SPIE, Vol 1601, pp.313-324,1990.

22. T. P. Hughes; Plasmas and laser light, John Wiley & Sons, New York, 1975.

23. C. M. Banas; High power laser welding'78, Optical Engineering, Vol 17, 1978.

24. D. A. Cremers, etc.; Direct laser-materials interaction, High temperature science,

Vol.27 pt 2, 1988-1989.

25. M. K. Chun and K. Rose; Interaction of high-intensity laser beams with metals, Journal of applied physics, Vol 41, 1970.

26. R. E. Mueller and W. W. Duley; Laser-liquid interactions under reduced gravity conditions, Microgravity Workshop, Ottawa, Canada, May 1990.

27. W. W. Duley; A summary of beam material interactions during laser processing, Proceedings of LAMP'87, Osaka, May, 1987.

28. Y. Arata, N. Abe and T. Oda; Fundamental phenomena in laser welding, pp.61-72, Inst. Phys. Conf., Ser. No.72, 1984.

29. I. Miyamoto, H. Maruo and Y. Arata; The role of gas assist in CO_2 laser welding, pp.68-75, ICALEO, 1984.

30. H. C. Peebles and R. L. Williamson; the role of the metal vapour plume in pulsed Nd:YAG laser welding on aluminum 1100, Proceedings of LAMP'87, Osaka, May, 1987.

31. T. Zacharia, S. A. David, J. M. Vitek and T. DebRoy; Weld pool development during GTA and laser beam welding of type 304 stainless steel, part 1--theoretical analysis, Welding Journal, p499s-509s, Dec. 1989.

32. R. S. Patel and M. Q. Brewster; Effect of oxidation and plume formation on low power Nd-Yag laser metal interaction, Journal of heat transfer, pp170-177, Vol.112, 1990.

33. R. Castro, J. J. de Cadenet; "Welding metallurgy of stainless and heat-resisting steels", the syndics of the Cambridge University Press(1975).

34. T. Lan, T. H. North: Fusion welding of stainless steels, Canadian Metallurgical Quarterly, Vol.27, No. 1, pp65-77, 1988.

35. P. A. A. Khan, T. DebRoy and S. A. David; Laser beam welding of high-manganese stainless steels--Examination of alloying element loss and microstructural changes, Welding Journal, pp.1s-7s, Jan.1988.

36. R. Uratani and A. Poli; I.I.W. Doc. IV-335-83.

37.M. Koso, M. Muira and N. Yamauchi; I.I.W. Doc. IV-418-86.

38. R. J. Coyle, Jr.; A microstructural study of pulsed and continuous laser welded stainless steel, Lasers in materials processing, ASM, 1983.

39. M. Bousseau, J. -M. Signamarcheix: Examples of possibilities offered by high power lasers in welding applications, ICALEO, 1986.

40.P.Y. Luciani, C. Charissoux; CO_2 laser auxiliary source couplings--application to welding, bibd. pp117-123.

41. K. N. Tandon, F. Saadat, et al.; Microgravity effects on directionally solidified castings(ground based experiments on Al-4%Cu alloys), Microgravity sci. technol. IV/1, pp.19-25, 1991.

42. F. Rosenberger, et al.; Influence of residual gravity on crystal growth processes, bibd. III/3, pp162-164, 1990.

43. N. V. Stoichev, et al.: Microgravity influence on the eutectic solidification in the presence of impurities, bibd, II/4, pp181-185, 1990.

44. C. Barta, et al.: Directional solidification of the PbCl2-AgCl eutectic system under various gravitational conditions, bibd. IV/1, pp26-31, 1991.

46. R. K. Crouch; Microgravity science and applications projects and payloads, Winter Annual meeting of ASM, 1987.

47. K. N. Tandon, J. R. Cahoon and M. C. Chaturvedi; Laser welding of alloys in microgravity environment-assessment of metallurgical characteristics, Proposal to MPB Technologies, July 1990.

48. M. Hans, and Joachim J. Schmidt; Influence of thermal gravitational convection on solidification processes, Mat. Res. Soc. Symp. Proc. Vol. 87. 1987.

49. H. J. Willenberg; Commercial materials processing in the space station, ASM 1987.

50. T. D. McCay, ect; Microgravity Science & Technology, v1/1, 1993.

51. M. H. McCay, ect; Metallurgical Transactions, Vol14A, pp.2163, 1983.

52. J. K. Watson, D. W. Dickinson; The role of welding in space maintenance and repair, Proceedings of space'88, New Mexico, 29-31, Aug. 1988.

53. R. M. Rivett; Welding in space--an overview, Winter Annual meeting of ASM, 1987.

54. T. DebRoy; Interfacial chemistry in welding, TWR'90, 1990.

55. W. F. Savage, C. D. Lundin and A. H. Aronson; Weld metal solidification mechanics, Welding Journal, pp.175s-181s, April 1965.

56. J. C. Lippold and W. F. Savage; Solidification of austenitic stainless steel weldments: Part 1- A proposed mechanism, Welding Journal, pp362s-374s, Dec. 1979.

57. J. C. Lippold and W. F. Savage; Solidification of austenitic stainless steel weldments: Part 2-The effect of alloy composition on ferrite morphology, Welding Journal, pp48s-58s, Feb. 1980.

58. S. A. David; Ferrite morphology and variations in ferrite content in austenitic stainless steel welds, Welding Journal, pp63s-71s, April 1987.

59. N. Suutala, T. Takalo and T. Moisio; Ferrite-austenitic stainless steel welds,

Metallurgical transactions A, Vol.11A, May 1980.

60. N. Suutala, T. Takalo and T. Moisio; The relationship between solidification and microstructure in Austenitic and austenitic-ferrite stainless steel welds, Metallurgical transactions A, Vol.10A, April 1979.

61. C. R. Loper, Jr., L. A. Shideler and J. H. Devletian; The effect of heat-affected zone structure on the structure of the weld fusion zone, Welding Journal, pp.171s-178s, April 1969.

62. J. F. Lancaster; Metallurgy of Welding, 3rd ed. George Allen &Unwin Ltd., 1980.

63. B. Chalmers; Physical Metallurgy, John Wiley & Sons, Inc., New York, p235, 1962.

64. S. Kou; Grain structure development in the fusion zone, TWR'89, 1989.

65. S. Kou and Y.H. Wang; Weld pool convection and its effect, Welding Journal, Vol.65, p63s, 1986.

66. S. A. David and J. M. Vitek; Proc. of TWR'92, pp.147-156, 1992.

67. J. A. Brooks and M. I. Baskes; Microsegregation modelling and transformation in rapidly solidified austenite stainless steel welds, TWR'89, 1989.

68. S. A. David, J. M. Vitek and T.L Hebble; Welding Journal, Vol.65, pp.289s-300s, 1987.

69. T. Zacharia, S. A. David, J. M. Vitek and T. DebRoy; Metall. Trans., Vol 20A, pp.957-967, 1989.

70. P. Sahoo, T. DebRoy and M. J. McNallan; Metall. Trans. Vol. 19B, p.483, 1988.

71. A. Paul, and T. DebRoy; Metallurgical Transactions, Vol.19B, pp.851-858, 1988.

72. G. M. Oreper and J. Szekely; Heat and fluid flow phenomena in weld pools, Journal

of Fluid Mechanics, Vol.147, p.53, 1984.

73. H. E. Cline and T. R. Anthony; Heating and melting material with a scanning laser or electron beam, Journal of applied physics, Vol.48, No.9 Sept. 1977.